

Time scales and processes of Cordilleran batholith construction and high-Sr/Y magmatic pulses: Evidence from the Bald Mountain batholith, northeastern Oregon

Joshua J. Schwartz^{1,*}, Kenneth Johnson², Paul Mueller³, John Valley⁴, Ariel Strickland⁴, and Joseph L. Wooden⁵

¹Department of Geology, California State University, Northridge, 18111 Nordhoff Street, Northridge, California 91330, USA

²Department of Natural Sciences, University of Houston-Downtown, Houston, Texas 77002, USA

³Department of Geological Sciences, University of Florida, Gainesville, Florida 32611, USA

⁴WiscSIMS (Wisconsin Secondary Ion Mass Spectrometer Laboratory), Department of Geoscience, University of Wisconsin, 1215 W. Dayton Street, Madison, Wisconsin 53706, USA

⁵School of Earth Sciences, Stanford University, Stanford, California 94305, USA

ABSTRACT

Cordilleran granitic batholiths (*sensu lato*) preserve information about time scales and processes of upper crustal magmatic arc construction during Mesozoic subduction and mountain building. The Bald Mountain batholith in northeastern Oregon (USA) is a classic example of a composite, incrementally constructed batholith that formed during terrane amalgamation outboard of the western U.S. Cordillera. Whole-rock geochemistry and zircon trace element, U-Pb, Lu-Hf, and O isotopic data reveal that batholith construction occurred over ~15 Ma, commencing with the syncollisional emplacement of small, low-Sr/Y (<40) norite-granite plutons from 157 to 155 Ma. The next phase of magmatism was postcollisional and dominated by high-Sr/Y (>40) tonalite-granodiorite magmatism that produced the main mass of the batholith, including the granodiorite of Anthony Lake (147 Ma) and the tonalite of Bald Mountain (145–141 Ma). Zircons from the norite-granite suite display a narrow range in initial ϵ_{Hf} of 7.2–7.7 and elevated $\delta^{18}\text{O}$ (Zrn) ranging from 8.2‰ to 10.0‰ (excluding one outlier). Zircons from the later granodiorite-tonalite suite show a similar range of initial ϵ_{Hf} values (6.3–8.9) and $\delta^{18}\text{O}$ (7.1‰–10.0‰), indicating a similar history of interaction with evolved crustal material. Modeling of whole-rock and zircon geochemistry indicates that both the low- and high-Sr/Y magmas composing the main phase of the batholith were generated by dehydration–partial melting of mafic arc

crust (e.g., amphibolite), leaving behind a plagioclase-poor restite, which was garnet granulite in the case of the high-Sr/Y magmas. Final magma compositions in both suites were affected by assimilation of supra-crustal material either at depth or during ascent. We suggest that high-Sr/Y magmas in the Bald Mountain batholith were generated by partial melting of thickened arc crust ~10 m.y. after arc-arc collision began at 159–154 Ma. Heat to drive lower crustal melting was conveyed by an increase in mantle power input as a result of renewed subduction-related magmatism. Mixing and homogenization in the lower crust involving mantle-derived basalts and crustally derived partial melts can account for the geochemical variation we observe in tonalites and granodiorites in the Bald Mountain batholith.

INTRODUCTION

Granitic batholiths (*sensu lato*) of the western U.S. Cordillera preserve a record of magmatic processes that operated at shallow- to mid-crustal depths during Mesozoic subduction and mountain building (Gromet and Silver, 1987; Bateman, 1992; Ducea, 2001; Saleeby et al., 2008; Lackey et al., 2005; Lee et al., 2006; Ducea and Barton, 2007; Miller et al., 2007; DeCelles et al., 2009; Memeti et al., 2010; Pater-son et al., 2011; Cecil et al., 2012). In continental magmatic arcs, granitic batholiths are commonly viewed as frozen manifestations of large silicic magma systems that once formed above subduction zones. As such, granitic batholiths record information about elusive features of large, subduction-related silicic magmatic systems such as the rates and time scales of mag-

matic processes including transport, storage, and solidification of magmas in subterranean reservoirs (Miller and Paterson, 2001; Mahan et al., 2003; Coleman et al., 2004; Glazner et al., 2004; Matzel et al., 2006; de Silva and Gosnold, 2007; Lipman, 2007; Bachman et al., 2007; Miller et al., 2007; Walker et al., 2007). Deconvolving the time scales over which plutons and batholiths are emplaced and the processes involved in their generation is critical to understanding the dynamics of crustal growth in continental magmatic arcs.

An increasing number of studies of volcanic and plutonic rocks have demonstrated that the growth of individual magma systems takes place incrementally over a variety of time scales (cf. Bacon et al., 2000; Reid and Coath, 2000; Vazquez and Reid, 2002; Schmitt et al., 2003; Coleman et al., 2004; Glazner et al., 2004; Oberli et al., 2004; Bacon and Lowenstern, 2005; Matzel et al., 2006; Bachmann et al., 2007; Walker et al., 2007; Barth et al., 2012; Reid, 2014). For example, Coleman et al. (2004) showed that the Tuolumne Intrusive Suite in the Sierra Nevada was constructed by emplacement of relatively small increments of magma over a period of 10 m.y. In the Mount Stewart batholith, the time of pluton assembly was also long, taking place over 5 m.y. (Matzel et al., 2006). However, in the Torres del Paine pluton in Patagonia, Michel et al. (2008) used high-precision chemical abrasion thermal ionization mass spectrometry zircon geochronology to document multiple pulses of magma emplacement over 90 ± 40 ka. Barboni and Schoene (2014) demonstrated that the transition from eruptible magma to solidification occurred in 10–40 k.y. These remarkably brief durations for pluton growth documented by Michel et al. (2008) and

*Email: joshua.schwartz@csun.edu.

Barboni and Schoene (2014) are similar to time scales of volcanic magma-chamber recharge and storage that are 0.1–100 k.y. (e.g., Reid et al., 1997; Brown and Fletcher, 1999; Miller and Wooden, 2004; Vazquez and Reid, 2004; Bacon and Lowenstern, 2005; Charlier et al., 2005; Bachmann et al., 2007; Reid, 2014).

Studies of large silicic volcanic fields that commonly form during ignimbrite flare-ups also provide insights into the construction of granitic batholiths in the shallow to middle crust (de Silva and Gosnold, 2007; Lipman, 2007). Voluminous eruptions of silica-rich magma during caldera-forming eruptions provide unequivocal evidence for the existence of large magma chambers (100–1000 km³), although direct geochemical and geophysical links between large plutons and silicic ignimbrites remain tentative (Lipman, 2007; Glazner et al., 2008). In the Altiplano-Puna volcanic complex, de Silva and Gosnold (2007) inverted erupted volumes and eruption durations to calculate the size and emplacement history of a putative subsurface granodiorite batholith that likely formed during the 1–10 m.y. ignimbrite flare-up; their results indicated that composite upper crustal batholiths can form episodically over several millions of years during flare-up events. These results from the Altiplano-Puna volcanic complex are remarkably similar to documented high-volume magmatic pulses in the Mesozoic Sierra Nevada batholith, where nearly 78% of the magmatic volume of the exposed arc was emplaced from ca. 100 to 85 Ma (Ducea, 2001). These studies of large silicic magma systems highlight the non-steady-state character of magmatism in arc settings whereby episodic and relatively short-lived, high-volume magmatic events significantly contribute to the overall budget of new crust added to the continental lithosphere (Kimbrough et al., 2001; Ducea, 2002; Ducea and Barton, 2007; de Silva and Gosnold, 2007; DeCelles et al., 2009). Such catastrophic and transient events can be triggered by an increase in mantle power and/or underthrusting of fertile continental crust, and can exert primary controls on orogenic belts, including widespread thermal and mass transfer from the mantle to the crust, vertical uplift and exhumation, and erosion at the surface.

In the Blue Mountains province of northeastern Oregon, silicic plutonic rocks intruded island-arc crust during and following lateral terrane collisions, providing a window into the time scales and processes of batholith generation along a tectonically active continental margin. Recent U-Pb zircon geochronology of plutonic rocks coupled with volcanic stratigraphy of adjacent basins indicates that Mesozoic arc magmatism involved eruptions of mafic-

intermediate magmas and emplacement of small plutons from ca. 190 to 154 Ma (Dickinson, 1979; Schwartz et al., 2011a, 2011b). This phase of magmatism terminated with a widespread, regional contraction event linked to the collision of the distal Wallowa island-arc terrane with the fringing Olds Ferry island-arc terrane (Schwartz et al., 2011a). Subsequent magmatism involved a transient pulse of silicic magmas emplaced during a brief interval from 148 to 140 Ma. Exhumed plutons and batholiths that formed during this pulse are dominantly tonalite to granodiorite in composition, and are geochemically characterized by elevated Na, Al, and Sr concentrations, and depletions in Y and heavy rare earth elements. These geochemical features are observed in so-called high-Sr/Y plutons and batholiths in convergent margins worldwide (e.g., Fiordland, New Zealand; Peninsular Ranges, USA; Cordillera Blanca, Peru; eastern Blue Ridge, USA; south Tibetan adakites in the Tibetan Plateau; e.g., Petford and Atherton, 1996; Tulloch and Kimbrough, 2003; Chung et al., 2003; Ingram, 2012), and represent a poorly understood phase of high-Sr/Y magmatism associated with continental crust construction along the western margin of the U.S. Cordillera.

The Bald Mountain batholith in the Blue Mountains province is a classic example of an incrementally constructed, composite Cordilleran batholith. Detailed field-based studies of the batholith over more than 45 years have documented a diverse suite of nested plutons, ranging in composition from norite to granite, that stitch accreted island-arc crust of the Wallowa island arc and Baker oceanic mélange terranes (Fig. 1; Taubeneck, 1957, 1995). This classic Cordilleran stitching batholith was constructed in a complexly faulted terrane boundary, and the age of its emplacement postdates collisional orogenesis in the region. Along its periphery, the batholith consists of several small mafic to felsic plutons; however, the interior of the batholith contains a large, compositionally zoned core of high-Sr/Y tonalite and granodiorite, which largely lacks internal intrusive contacts. Here we use a combination of whole-rock geochemistry, U-Pb zircon geochronology, and trace element and Hf-O isotope geochemistry of zircon to investigate time scales and processes of magma generation and composite Cordilleran batholith construction. Our results suggest that the Bald Mountain batholith was constructed over a 15 m.y. interval in 2 distinct episodes that span a period of terrane collision and plate reorganization along the western U.S. Cordillera. These two pulses involved (1) syncontractional emplacement of small, low-Sr/Y plutons at 157–155 Ma, and (2) postdeformational emplacement dominated

by large, high-Sr/Y plutons from 147 to 141 Ma. We propose a model whereby low-Sr/Y plutons were generated by crystallization of hybrid, subduction-related mantle melts and/or melting of amphibolites at moderate pressure (<1.0 GPa) during the waning stages of subduction and terrane amalgamation. In contrast, the transient pulse of high-Sr/Y magmatism was triggered by an increase in mantle power that resulted in partial melting of orogenically thickened island-arc crust during a renewed phase of subduction-related magmatism. Our results from the Bald Mountain batholith highlight temporally evolving processes of low- and high-Sr/Y magmatism, crustal thickening, and the geochemical maturation of arc crust associated with terrane collisions and plate reorganization over a 15 m.y. interval along the western U.S. Cordillera.

GEOLOGIC BACKGROUND

The Blue Mountains province of northeastern Oregon and western Idaho (Fig. 1) is a complex collage of island-arc and related mélange and/or sedimentary terranes that accreted to western North America in the Early Cretaceous (Selverstone et al., 1992; Getty et al., 1993; McKay, 2011). Terranes of the Blue Mountains province consist of the Permian to Early Jurassic Wallowa island arc, the Middle Triassic to Early Jurassic Olds Ferry island arc, the Permian to Early Jurassic Baker oceanic mélange terrane, and the Late Triassic to Late Jurassic Izee forearc-collisional basin (Brooks and Vallier, 1978; Dickinson and Thayer, 1978; Dickinson et al., 1979; Silberling et al., 1987; LaMaskin et al., 2009; Schwartz et al., 2010, 2011a). All terranes of the Blue Mountains province were faulted and folded during a widespread north-south-directed contractional event between 159 and 154 Ma, interpreted to record a short-lived episode of deformation related to the terminal collision of the distal Wallowa island arc with the fringing Olds Ferry island arc (cf. Figs. 2A–2C; Avé Lallement, 1995; Ferns and Brooks, 1995; Schwartz et al., 2010, 2011a). Jurassic to Cretaceous magmatic activity in the region occurred during three main phases: (1) ca. 190–154 Ma; (2) 148–141 Ma; and (3) 133–118 Ma (Johnson and Schwartz, 2009; Schwartz et al., 2011b). The terminal portion of the ca. 190–154 Ma phase overlapped with contractional deformation, whereas the 148–141 Ma phase is characterized by postcontractional tonalite-granodiorite plutonism. A zircon age from a gabbro-norite in an unspecified location within the Bald Mountain batholith yielded an age of ca. 143 Ma (no uncertainties given), suggesting that the batholith formed in part during the postcontractional phase (Walker, 1989).

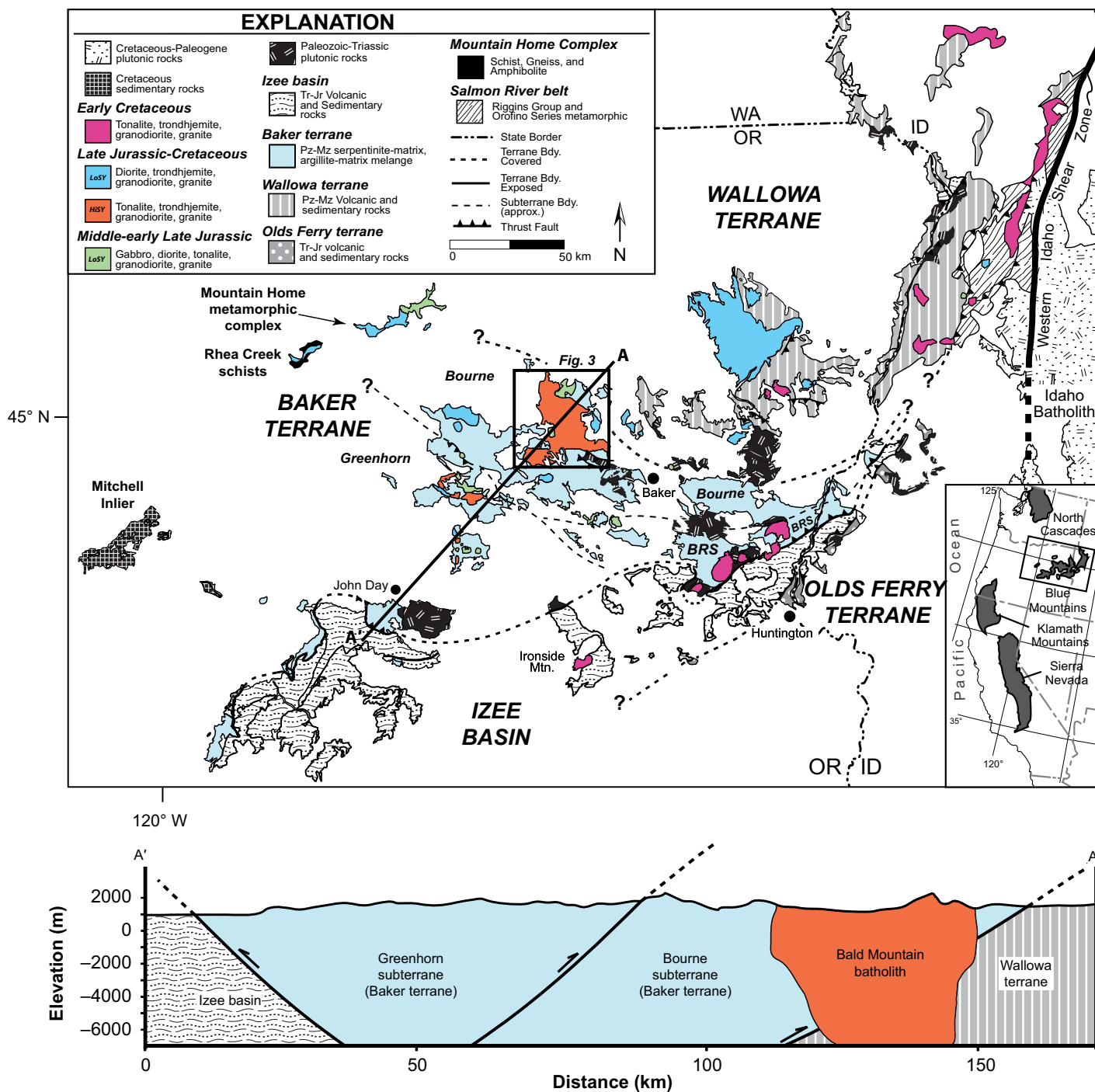


Figure 1. Regional map of the Blue Mountains province, northeastern Oregon and western Idaho, showing the locations of the various terranes and subterranean (modified from LaMaskin et al., 2009). A–A' refers to cross section below regional map. Location of Figure 3 is shown for reference. Inset map shows location of the Blue Mountains province with respect to other Paleozoic–Mesozoic accreted terranes and Jurassic to Cretaceous magmatic rocks of the North American Cordillera. BRS—Burnt River Schist (Ashley, 1995).

Wall Rocks Surrounding the Bald Mountain Batholith

The Bald Mountain batholith intrudes the structurally complex boundary between the Baker oceanic mélangé terrane (Bourne

subterranean) and the Wallowa island-arc terrane (cf. Figs. 1 and 2C). In this complex fault zone, the Wallowa-Baker terrane boundary consists of a series of imbricated slabs of metaigneous rocks derived from the Wallowa island arc that were faulted into Early Jurassic to Permian Elk-

horn Ridge Argillite of the Baker terrane along low- to moderately southward-dipping thrust faults (cf. Ferns and Brooks, 1995; Schwartz et al., 2010, 2011a). Host rocks to the batholith include chert, argillite, limestone, and tuffaceous argillite of the Elkhorn Ridge Argillite

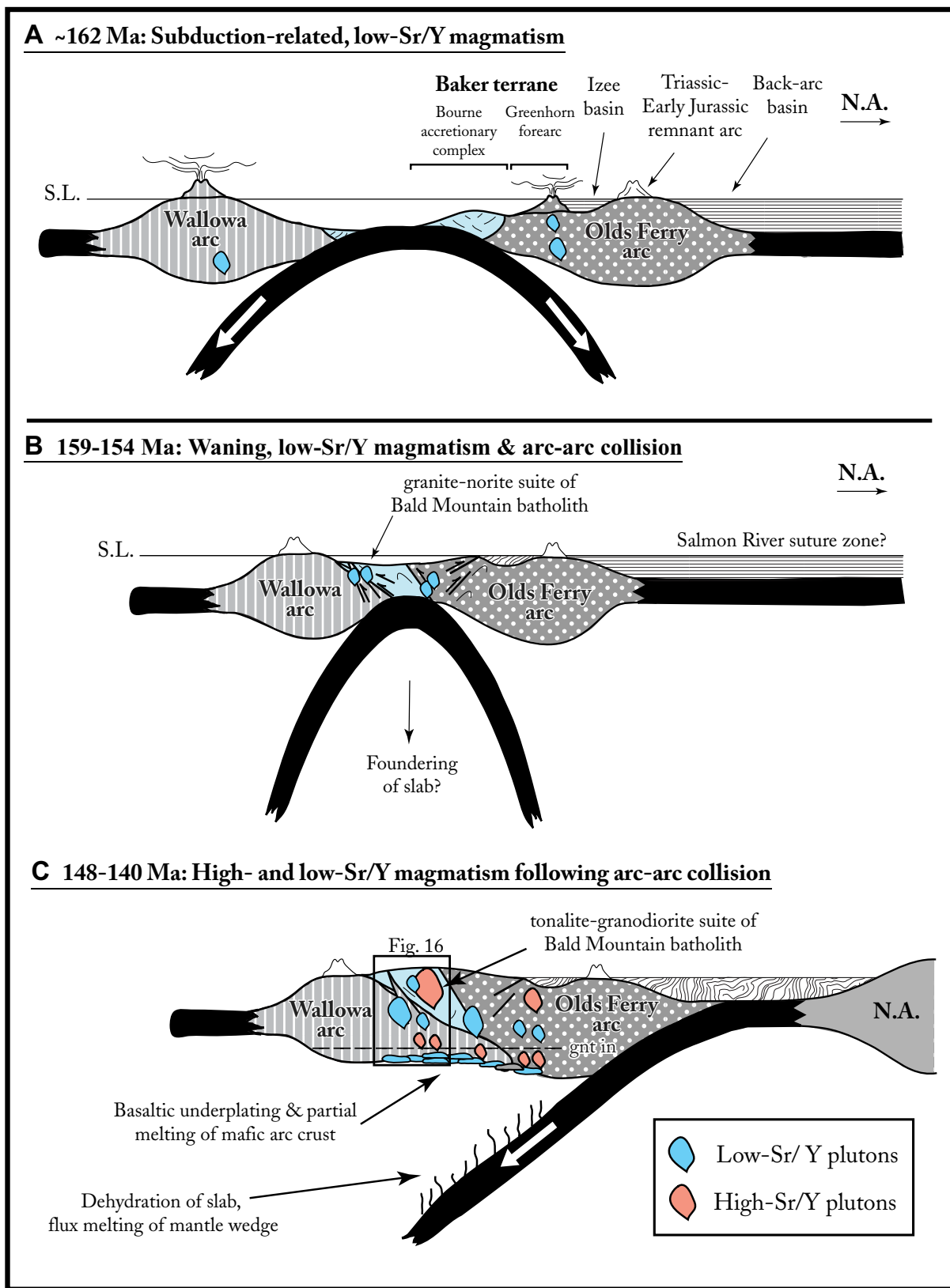


Figure 2. Schematic models for the evolution of the Blue Mountains province and the Bald Mountain batholith (after Schwartz et al., 2011b). (A, B) Doubly vergent subduction resulted in low-Sr/Y magmatism in both the Olds Ferry and Wallowa island-arc systems. S.L.—sea level; N.A.—North America. (C) Following regional contraction at 159–154 Ma, high-Sr/Y plutons formed in the orogenically thickened regions of the Baker terrane (gnt—garnet).

and hornblende metagabbros of the Wallowa island arc (Taubeneck 1957, 1995). Metagabbros are Triassic (241–225 Ma; Walker, 1995; Schwartz et al., 2010) and similar to rocks reported from other areas of the Wallowa terrane (Kurz et al., 2012). Pervasive, regional, greenschist facies metamorphism affected both Elkhorn Ridge Argillite and metagneous units prior to batholith emplacement (Ferns and Brooks, 1995; Schwartz et al., 2010). The $^{87}\text{Sr}/^{86}\text{Sr}$ values for the Elkhorn Ridge Argillite range from 0.7113 to 0.7128, and from 0.7032 to 0.7036 for the metaplutonic thrust slices (recalculated to 147 Ma using data reported in Schwartz et al., 2010). Calculated ϵNd values for the Elkhorn Ridge Argillite at 147 Ma range from -6.9 to -10.0 , and from $+5.7$ to $+7.6$ for the metaplutonic thrust slices (using data reported in Schwartz et al., 2010).

Contact metamorphic mineral assemblages locally replace greenschist facies minerals in the Elkhorn Ridge Argillite and metagabbro thrust slices in the contact aureole. Relict greenschist facies mineral assemblages in the Elkhorn Ridge Argillite (outside the aureole) consist of quartz + plagioclase + carbonate \pm chlorite \pm white mica. Within the metamorphic aureole, mineral assemblages are quartz + plagioclase + biotite \pm garnet \pm cordierite \pm orthoclase \pm rutile \pm andalusite \pm sillimanite).

Bald Mountain Batholith: Norite-Granite Suite

The Bald Mountain batholith comprises a diachronous plutonic suite. The batholith was extensively mapped by Taubeneck (1957, 1995) and consists of two igneous suites: an older, mafic-felsic suite of lesser areal extent and a younger, laterally extensive, tonalite-granodiorite suite (Fig. 3). The older suite includes norite, quartz diorite, and granite. Mafic units include two small intrusions (norite of Willow Lake and quartz diorite of Black Bear) and one larger unit termed the norite of Badger Butte, which has an area of ~ 6.5 km². Primary minerals in the norite of Badger Butte include plagioclase, hypersthene, augite, and minor quartz, hornblende, biotite, sphene, and zircon. In contrast to the tonalite-granodiorite suite, the norite of Badger Butte displays extensive silicic and pyritic alteration. Subsidiary deformational fabrics are characterized by recrystallization of plagioclase feldspar and microfracturing of pyroxene (see Taubeneck, 1957, 1995, for detailed descriptions of these units). One Rb-Sr analysis of the norite of Willow Lake by Armstrong et al. (1977) yielded an initial $^{87}\text{Sr}/^{86}\text{Sr}$ value of 0.7037 (recalculated assuming 156 Ma crystallization and $\lambda^{87}\text{Rb} = 1.42 \times 10^{-11}\text{yr}^{-1}$). Only xenoliths of Elkhorn

Ridge Argillite are reported in the norite-granite suite (Taubeneck 1957, 1995).

Felsic plutonic components of the older suite crop out along the northeastern margin of the batholith and include the granite of Anthony Butte and the quartz diorite of Wolf Creek. The granite of Anthony Butte extends over ~ 16 km², making it the largest granitic pluton in northeastern Oregon at the present level of exposure. It intrudes the quartz diorite of Wolf Creek on its northern margin and Elkhorn Ridge Argillite to the east. Primary accessory minerals include biotite, sphene, and zircon, and rare garnet, orthopyroxene, and cummingtonite. Subsidiary deformation is common in this unit and characterized by weak to strong undulose quartz, sutured quartz grain boundaries, microfracturing of plagioclase, and mineral alignment of biotite and potassium feldspar. The quartz diorite of Wolf Creek occupies an area of ~ 4.5 km². It is intruded by the granite of Anthony Butte, making it one of the oldest units in the northeastern section of the Bald Mountain batholith. Primary minerals include plagioclase, potassium feldspar, quartz, hornblende, biotite, augite, orthopyroxene, apatite, and zircon. Quartz and plagioclase feldspar also display sutured grain boundaries and undulose extinction.

Bald Mountain Batholith: Tonalite-Granodiorite Suite

The most extensive unit of the batholith is the tonalite of Bald Mountain (tonalite-granodiorite suite), which makes up $>90\%$ of surface exposures (~ 344 km²). Taubeneck (1995) subdivided the tonalite of Bald Mountain into three units based on modal mineralogy: a northern augite-bearing, biotite-hornblende tonalite (located north of intraplutonic contact A-B; Fig. 3), a central biotite-hornblende tonalite, and a southern hornblende-biotite tonalite (located west of intraplutonic contact C-D in the Monument salient area; Fig. 3). Rocks north of intraplutonic contact A-B crop out over 18 km² and are distinguished by the presence of augite cores in hornblende, whereas augite is absent in tonalite elsewhere in the batholith. Subsidiary deformational fabrics characterized by recrystallized plagioclase and quartz are also common near the intraplutonic contact in this area. Tonalites of the Monument salient (southwestern portion of the batholith; Fig. 3) are distinctively more silicic than the rest of the batholith and contain, on average, higher modal percentages of quartz and biotite, and lesser amounts of hornblende. Gold mineralization in the Bald Mountain batholith is also primarily located in and around the Monument salient region (Ferns et al., 1982). Armstrong et al. (1977) reported initial $^{87}\text{Sr}/^{86}\text{Sr}$

values for the tonalite of Bald Mountain ranging from 0.7038 to 0.7043 (recalculated using new $^{206}\text{Pb}/^{238}\text{U}$ zircon ages reported here and $\lambda^{87}\text{Rb} = 1.42 \times 10^{-11}\text{yr}^{-1}$).

The core of the batholith consists of the granodiorite of Anthony Lake. It is exposed over ~ 88 km² and has gradational contacts with the tonalite of Bald Mountain, except along its northern and eastern margins, where it displays a sharper mineralogical contrast against crystal-plastically deformed tonalite (Taubeneck 1957, 1995). Elsewhere, boundaries between tonalite and granodiorite are largely based on modal abundances of potassium feldspar, whereby core granodiorites typically have potassium feldspar abundances $>4\%$ (see Taubeneck 1995, fig. 2.13 therein). A $^{206}\text{Pb}/^{238}\text{U}$ zircon age of 146.7 ± 2.1 Ma was reported for the granodiorite unit (Schwartz et al., 2011a). Recalculated initial $^{87}\text{Sr}/^{86}\text{Sr}$ values range from 0.7043 to 0.7044 and overlap with those from the tonalite of Bald Mountain (Armstrong et al., 1977).

Both the tonalite and granodiorite units contain abundant xenoliths of country rock extending well into the interior of the batholith. Xenoliths include, in order of increasing abundance, calc-silicate rocks, cherty argillite, ribbon chert, and foliated metagabbro. Length dimensions for the xenoliths range to 22 cm for calc-silicates, 51 cm for cherty argillites, 89 cm for ribbon cherts, and 31 cm for foliated metagabbros (Taubeneck, 1995). Xenoliths of chert and cherty argillite commonly display irregular and subrounded boundaries. Many xenoliths of cherty argillite also display halos of iron oxide. Whereas xenoliths of cherty argillite are relatively common in the contact aureole of the batholith, they are less common in the interior of the batholith compared to other compositions. Foliated metagabbro xenoliths show little evidence for reaction with host tonalite and granodiorite.

Mafic enclaves are also common in the tonalite-granodiorite suite and are more voluminous than xenoliths. Mafic enclaves range from undeformed fine-grained hornblende microdiorite to porphyritic hornblende andesite; no garnet is observed in any mafic enclaves. Mafic enclaves are distinguished from Permo-Triassic xenoliths in that they are non-foliated, commonly subrounded to rounded, and show no signs of greenschist-facies alteration. Mafic enclaves range from 2 to 30 cm in length. The estimated volume percent of mafic enclaves in tonalite and granodiorite ranges from 0.32% to 0.35% (Taubeneck, 1995). Most enclaves are subrounded in shape and are not associated with synplutonic mafic dikes, although they occasionally form swarms (e.g., 0.5 km northwest of Mt. Ireland; Taubeneck, 1995). Chilled margins on the rims of mafic enclaves are also observed.

Cordilleran batholith construction and high-Sr/Y magmatic pulses

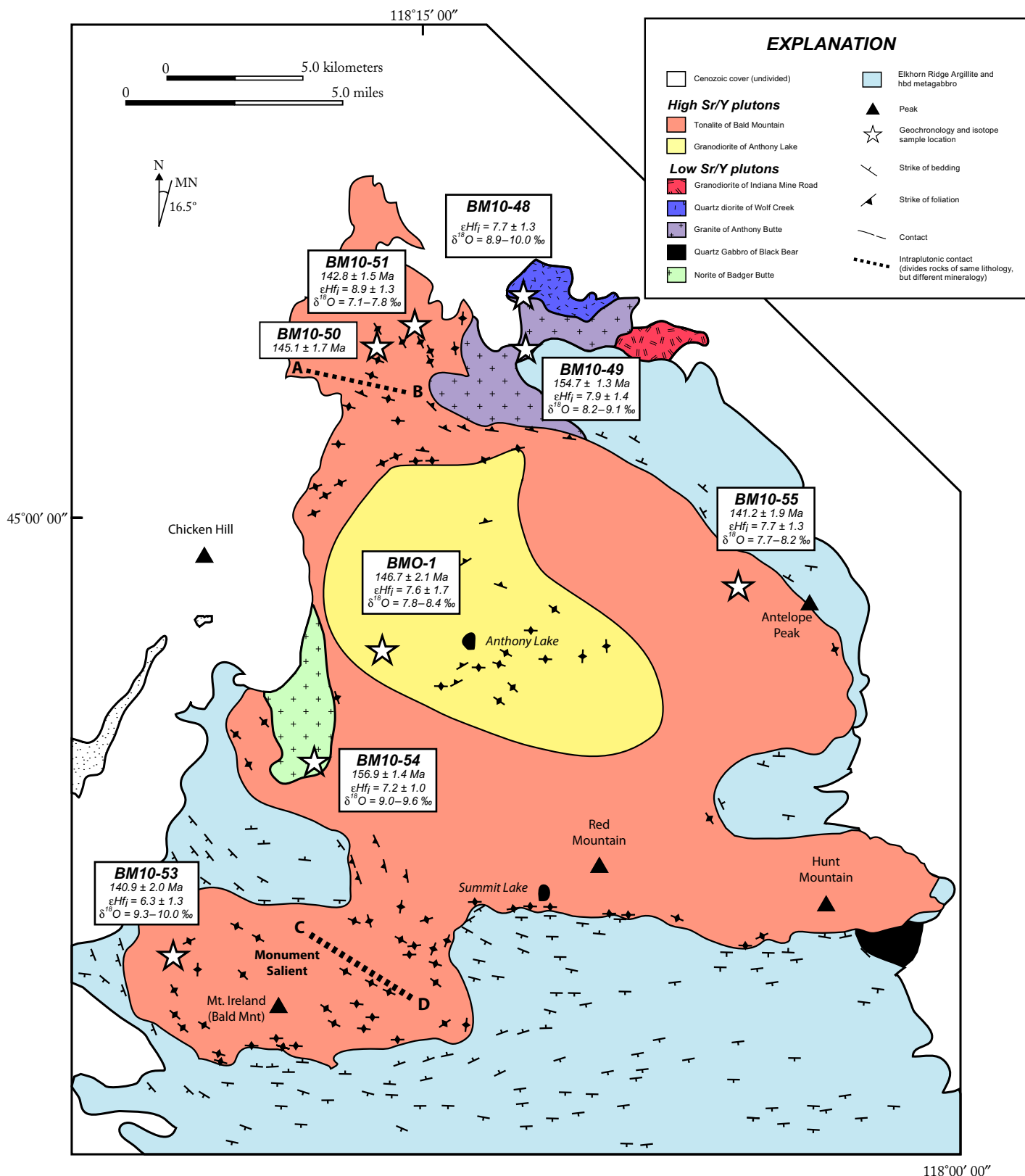


Figure 3. Simplified geologic map of the Bald Mountain batholith (after Taubeneck, 1995). Locations of samples discussed in text are shown by white stars along with zircon $^{206}\text{Pb}/^{238}\text{U}$ ages, average initial ϵ_{Hf} values, and range of $\delta^{18}\text{O}$ (Zrn) values. Zircon isotopic data are summarized in Table 3.

TABLE 1. SUMMARY OF GEOCHEMICAL AND ISOTOPIC DATA FROM THE BALD MOUNTAIN BATHOLITH, BLUE MOUNTAINS PROVINCE, NORTHEASTERN OREGON

Unit	Representative sample	Age (Ma)	Fe number (value)	MALI	ASI	SiO ₂ (range)	~Sr (average)	Sr/Y (average)	δ ¹⁸ O (WR) (average)	δ ¹⁸ O (Zrn) (average)	⁸⁷ Sr/ ⁸⁶ Sr initial* (WR)	εHf initial (Zrn) (average)
Norite of Badger Butte	BM10-54	156.9	magnesian (0.56–0.69)	calcic to calc-alkalic	metaluminous	48–58	574	23	8.5	9.3	¹⁰ 0.7037	7.2
Quartz diorite of Wolf Creek	BM10-48	>155	magnesian	calc-alkalic	peraluminous	71	178	8	n.d.	9.7	n.d.	7.7
Granite of Anthony Butte	BM10-49	154.7	magnesian to ferroan (0.72–0.78)	calc-alkalic	peraluminous	73–74	201	22	8.6	8.5	n.d.	7.9
Granodiorite of Anthony Lake enclaves	BMO-1	146.7	magnesian (0.65–0.70)	calcic	metaluminous	66–68	488	54	9.6	8.2	0.7043–0.7044	7.6
	BM-05-23B		magnesian (0.60–0.66)	calc-alkalic to alkali-calcic	metaluminous	54–59	475	13	n.d.	n.d.	n.d.	n.d.
Tonalite of Bald Mountain enclaves	BM10-53	140.9	magnesian (0.46–0.75)	calcic	metaluminous to peraluminous	51–71	510	47	11.1	9.7	0.7038–0.7043	6.3
	BM10-55	141.2								8.2		7.7
	BM10-51	142.8								7.5		8.9
	BM10-50	145.1								n.d.		n.d.
	BMB-2C		magnesian (0.59–0.67)	calc-alkalic	metaluminous	55–65	415	18	8.5	n.d.	n.d.	n.d.

Note: MALI—modified alkali lime index; ASI—aluminum saturation index; WR—whole rock; Zrn—zircon; n.d.—no data.

*Data from Armstrong et al. (1977).

[†]Norite of Willow Creek (Taubeneck, 1957; Armstrong et al., 1977).

METHODS

Samples for whole-rock geochemistry were collected from the principal units of the Bald Mountain batholith. Samples for U-Pb zircon geochronology, zircon trace element, and Lu-Hf and O isotopic analyses consist of three samples from the tonalite of Bald Mountain and single samples from the granodiorite of Anthony Lake, the norite of Badger Butte, the granite of Anthony Butte, and the quartz diorite of Wolf Creek. Major and trace element abundances were determined by inductively coupled plasma-atomic emission spectroscopy at Texas Tech University and the University of Houston-Downtown. Rubidium abundances were determined by atomic absorption spectrometry at Texas Tech University. Whole-rock oxygen isotope analyses were conducted at Texas Tech University and the University of Wisconsin-Madison. Plagioclase and hornblende mineral analyses were conducted at the University of Wyoming using the 5-spectrometer JEOL JXA-8900 electron microprobe. Zircons for geochronology and geochemical analyses were separated following standard methods involving density (Gemini table and heavy liquids) and magnetic (Frantz isodynamic separator) separation techniques at the University of Alabama. Zircons were mounted in epoxy, ground and polished, and imaged on a Gatan MiniCL detector attached to a JEOL 8600 electron microprobe analyzer at the University of Alabama. U-Pb zircon geochronology and trace element analyses were conducted at the U.S. Geological Survey–Stanford SHRIMP-RG (sensitive high-resolution ion

microprobe–reverse geometry) facility and the California State University Northridge LA-SF-ICP-MS (laser ablation–sector field–inductively coupled plasma–mass spectrometry) facility. Zircon Hf isotope geochemistry was performed by LA-MC-ICP-MS (MC—multicollector) at the University of Florida using a Nu Plasma MC-ICP-MS and a New Wave 213 nm laser. In situ zircon oxygen isotope ratios were measured at the University of Wisconsin-Madison using the Cameca IMS-1280 ion microprobe. Detailed descriptions of methods for whole-rock geochemistry, isotopic analysis, and sample locations are provided in the Supplemental File¹. Whole-rock and mineral geochemical data are reported in the Supplemental File (see footnote 1), and summarized in Tables 1 and 2.

RESULTS

Zircon Geochronology

Zircons from both the norite-granite and tonalite-granodiorite suites display well-developed oscillatory zoning with minor indications of xenocrystic cores and younger overgrowths (Fig. 4). Xenocrystic cores were avoided whenever possible during analysis. Rare Late Jurassic inherited zircons are most common in the tonalite suite and are shown by dashed error ellipses in Figure 5 (also see Table 3). These

¹Supplemental File. Zipped file containing detailed description of methods and supplemental figure and tables. If you are viewing the PDF of this paper or reading it offline, please visit <http://dx.doi.org/10.1130/GES01033.S1> or the full-text article on www.gsapubs.org to view the Supplemental File.

analyses are excluded in error-weighted average age calculations. No Mesozoic or older detrital zircons characteristic of the Elkhorn Ridge Argillite were observed. Representative cathodoluminescence images for zircons from the norite-granite and tonalite-granodiorite suite are shown in Figure 4 along with Pb/U, Hf, and O spot locations and isotopic results. Data are also summarized in Table 3.

The oldest unit in the Bald Mountain batholith is the norite of Badger Butte. Individual SHRIMP-RG spot analyses of 10 separate zircons yield an error-weighted average ²⁰⁶Pb/²³⁸U age of 156.9 ± 1.4 Ma (mean square of weighted deviates, MSWD = 0.8; Fig. 5A). One spot analysis is slightly older (164 Ma) than the majority of the analyses and likely represents a xenocryst. One zircon yields a younger apparent age of 146 Ma, and likely underwent minor Pb loss. Concordant SHRIMP-RG spot analyses (n = 11) from the granite of Anthony Butte give an error-weighted average ²⁰⁶Pb/²³⁸U age of 154.7 ± 1.3 Ma (MSWD = 1.0; Fig. 5B).

Two tonalite of Bald Mountain samples were collected from the northern pluton, and one sample was collected from each of the central and southwestern regions (Figs. 3 and 5C–5F). Eight individual SHRIMP-RG spot analyses from eight separate zircons from a northern tonalite (BM10-51) yield an error-weighted average ²⁰⁶Pb/²³⁸U age of 142.8 ± 1.5 Ma (MSWD = 0.6). Three spot analyses from three other zircons give older dates ranging from 146.3 to 147.5 and are likely xenocrysts from the granodiorite of Anthony Lake (146.7 ± 2.1 Ma; Schwartz et al., 2011a).

TABLE 2. REPRESENTATIVE WHOLE-ROCK MAJOR AND TRACE ELEMENT GEOCHEMICAL DATA

	Tonalite of Bald Mountain			Granodiorite of Anthony Lake	Norite of Badger Butte	Granite of Anthony Butte	Quartz diorite of Wolf Creek
	BM10-50	BM10-53	BM10-55	BMgd	BM10-54	BM10-49	BM10-48
SiO ₂	53.81	63.79	68.53	66.37	46.38	72.61	71.12
TiO ₂	0.82	0.61	0.33	0.51	1.01	0.10	0.18
Al ₂ O ₃	13.88	17.09	15.45	16.17	18.97	14.16	14.33
FeO*	8.71	4.09	2.53	4.55	9.01	1.13	1.22
MnO	0.16	0.08	0.06	0.08	0.17	0.04	0.05
MgO	8.09	1.90	1.26	2.01	5.85	0.31	0.49
CaO	11.71	4.87	3.78	4.31	10.64	1.64	1.90
Na ₂ O	1.97	4.13	4.13	4.04	2.86	3.87	3.33
K ₂ O	0.54	1.54	2.11	2.12	0.51	3.85	4.25
P ₂ O ₅	0.18	0.16	0.09	0.13	0.26	0.04	0.05
L.O.I.	1.38	0.61	0.50	n.d.	0.47	0.49	0.42
Total	101.25	98.88	98.77	100.29	96.13	98.25	97.33
Fe#	0.52	0.68	0.67	0.69	0.61	0.78	0.71
MAI	-9.21	0.81	2.46	1.85	-7.27	6.08	5.67
K ₂ O/Na ₂ O	0.27	0.37	0.51	0.52	0.18	1.00	1.28
Ba	394.0	840.5	868.7	832.0	415.6	1542.7	1173.8
Rb	5.8	34.9	44.8	48.0	4.8	55.4	132.1
Sr	392.0	625.2	463.5	479.0	509.3	218.9	178.3
Pb	2.9	6.0	8.5	n.d.	2.7	12.3	15.8
Th	1.5	1.8	4.9	n.d.	1.1	6.1	12.0
U	0.5	0.7	0.9	n.d.	0.3	0.7	7.6
Zr	48.6	22.6	32.9	110.0	44.3	39.7	69.3
Nb	12.9	17.1	12.5	8.0	24.9	18.7	31.9
Y	16.6	10.0	6.8	12.0	30.9	6.3	23.1
La	10.8	12.7	18.5	n.d.	15.7	22.8	29.8
Ce	24.6	24.4	29.6	n.d.	33.6	34.4	48.6
Pr	3.7	3.2	3.3	n.d.	4.8	3.6	5.5
Nd	17.2	13.3	11.8	n.d.	22.5	12.1	20.5
Sm	3.8	2.3	1.5	n.d.	5.5	1.3	3.7
Eu	1.0	0.7	0.5	n.d.	1.6	0.2	0.4
Gd	n.d.	n.d.	n.d.	n.d.	n.d.	n.d.	n.d.
Tb	0.5	0.3	0.2	n.d.	0.9	0.2	0.6
Dy	3.1	1.9	1.3	n.d.	6.0	1.3	4.1
Ho	0.6	0.4	0.2	n.d.	1.2	0.2	0.8
Er	1.7	1.0	0.6	n.d.	3.4	0.5	2.3
Tm	0.2	0.1	0.1	n.d.	0.5	0.1	0.4
Yb	1.6	0.9	0.7	n.d.	3.1	0.5	2.6
Lu	0.2	0.1	0.1	n.d.	0.4	0.1	0.4
Sc	45.0	7.7	6.0	10.0	33.9	3.5	5.4
V	221.7	85.8	57.7	84.0	266.8	10.1	15.3
Cr	149.7	11.8	16.2	19.0	35.1	2.3	7.8
Ni	70.1	5.5	377.9	15.0	18.1	1.3	2.5
Cs	1.9	1.0	1.0	n.d.	0.2	0.5	7.3
Sr/Y	23.7	62.6	68.3	39.9	16.5	34.5	7.7

Note: BM—Bald Mountain sample number; MAI—modified alkali lime index; n.d.—no data.

A second sample from the northern pluton (BM10-50) yields 24 concordant to slightly discordant LA-SF-ICP-MS spot analyses. The common-Pb corrected, error-weighted average age is 145.1 ± 1.7 Ma (MSWD = 1.5; Fig. 5D), which overlaps within error the SHRIMP-RG age of 142.8 ± 1.5 Ma from the nearby northern tonalite sample BM10-51. Five additional laser spot analyses from five zircons in BM10-50 indicate older dates ranging from 158.5 to 153.9 Ma and give an error-weighted average age of 155.6 ± 2.8 Ma (MSWD = 0.3). This minor, older population likely represents zircons inherited from the norite-granite suite dated in this study (154.7 ± 1.3 Ma to 156.9 ± 1.4 Ma).

Two samples from the central and southwestern regions of the tonalite of Bald Mountain yield SHRIMP-RG error-weighted average ages of 141.2 ± 1.9 Ma (MSWD = 1.0) and 140.9 ± 2.0 Ma (MSWD = 0.5), respectively. Both samples also contained older zircons with individual

spot dates of 149.7–146.6 Ma, similar to older, individual spot analyses observed in the northern tonalite (BM10-51).

WHOLE-ROCK GEOCHEMISTRY

Wall Rocks Surrounding the Bald Mountain Batholith

The Elkhorn Ridge Argillite ranges in composition from 74 to 83 wt% SiO₂ (Schwartz et al., 2010). It is characterized by low CaO (<0.5 wt%) and Sr (<300 ppm) concentrations, and low Sr/Y values (<25). Values of $\delta^{18}\text{O}$ (whole rock, WR) range from 22.0‰ to 27.6‰ (n = 9). Metagneous rocks occur as thrust slices of possible Wallowa island-arc affinity and have a broad range in SiO₂ content ranging from ~48–67 wt% (Ferns and Brooks, 1995; Schwartz et al., 2010). They also have high Al₂O₃ values (16.4–20.2 wt%) and moderate to high CaO

(3.8–10.2 wt%) and Sr concentrations (187–505 ppm). Values of $\delta^{18}\text{O}$ (WR) range from 11.2‰ to 14.5‰ (n = 5).

Norite-Granite Suite (157–155 Ma)

The norite-granite suite is bimodal in SiO₂ and is characterized by low average Sr/Y (<40), moderate to high average Sr (182–746 ppm), and high average Y (>15 ppm; Fig. 6). SiO₂ concentrations range from 48 to 58 wt% for the norite of Badger Butte and from 73 to 74 wt% for the granite of Anthony Butte. According to the three-tiered classification scheme of Frost et al. (2001), the norite of Badger Butte is magnesian, calcic, and metaluminous; the granite of Anthony Butte is magnesian to ferroan, calcic to calc-alkalic, and weakly peraluminous (Figs. 6A–6C). The norite of Badger Butte displays slight light rare earth element (LREE) enrichment, a small negative Eu anomaly, and flat heavy rare earth element (HREE) abundances (Fig. 7A). The quartz diorite of Wolf Creek is similar to the norite of Badger Butte, with the exception of a pronounced negative Eu anomaly. The granite of Anthony Butte displays more steeply fractionated REE patterns, and a pronounced negative Eu anomaly. Compared to normal mid-oceanic ridge basalt (NMORB), all three units display large ion lithophile element (LILE) enrichment, and strong positive Pb anomalies in normalized trace element plots (Fig. 7B). Whereas the granite of Anthony Butte and the quartz diorite of Wolf Creek display weak negative Nb anomalies, the norite of Badger Butte displays a slight positive anomaly. Average zircon and apatite saturation temperatures are 648 °C and 768 °C for the norite of Badger Butte, 709 °C and 865 °C for the granite of Anthony Butte, and 717 °C and 894 °C for the quartz diorite of Wolf Creek (Watson and Harrison, 1983; Harrison and Watson, 1984). Whole-rock $\delta^{18}\text{O}$ values for the norite of Badger Butte range from 8.4‰ to 10.4‰ (n = 4), whereas the granite of Anthony Butte yielded a $\delta^{18}\text{O}$ value of 10.6‰ (n = 1; see Supplemental File [see footnote 1]).

Tonalite-Granodiorite Suite (147–141 Ma)

Intrusive rocks that compose the majority of the Bald Mountain batholith (Elkhorn pluton of Taubeneck, 1957) are generally tonalitic to granodioritic in composition, although some samples are dioritic. For simplicity, we refer to all of these rocks as the tonalite-granodiorite suite. The tonalite-granodiorite suite has variable SiO₂ contents ranging from 52 to 71 wt%, and Mg# values ranging from ~39 to 70. All tonalites and granodiorites are magnesian, calcic, and metaluminous to weakly peraluminous (Figs. 6A–6C). Based on Sr/Y values, REE concentrations, modal mineralogy and

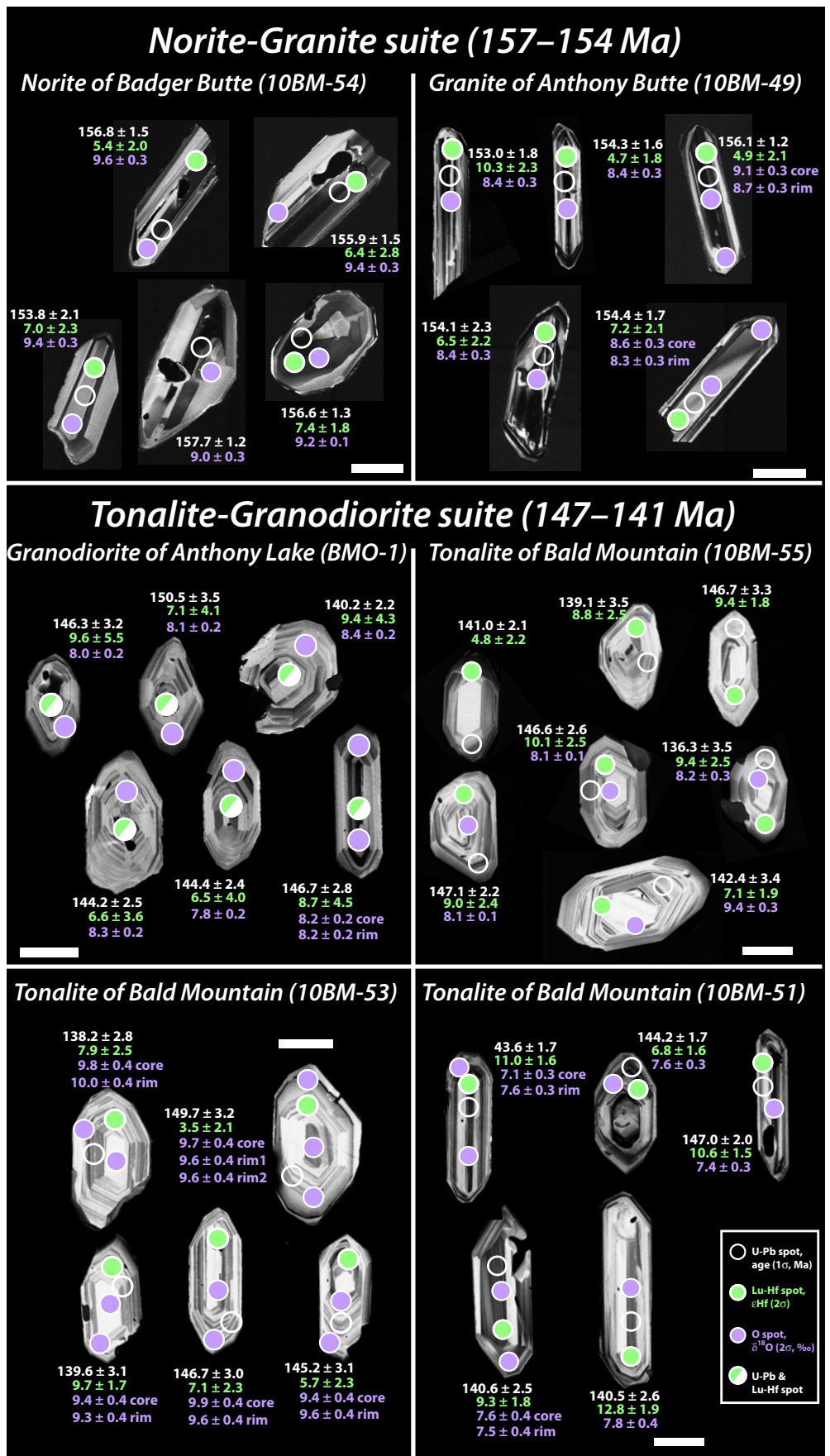


Figure 4. Representative cathodoluminescence images of zircons from the norite-granite and tonalite-granodiorite suites of the Bald Mountain batholith. Locations of ion microprobe and laser ablation spots are shown along with data from each spot. Analysis spots are color coded: white—U-Pb age, green—Lu-Hf, purple—O. Scale bars are 100 μm.

Cordilleran batholith construction and high-Sr/Y magmatic pulses

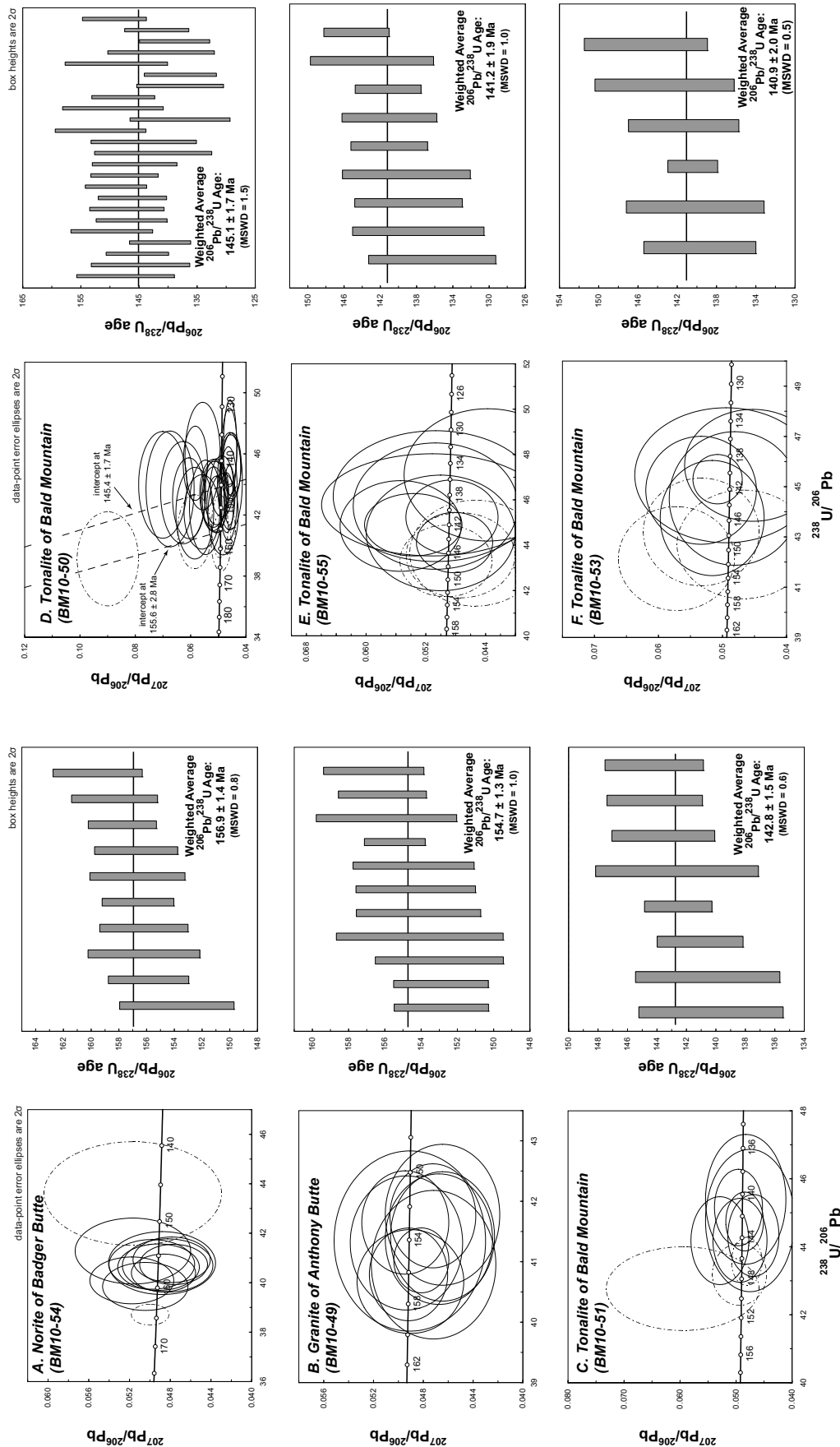


Figure 5. (A–F) Tera-Wasserburg diagrams and error-weighted average age plots for zircons from plutonic rocks of the Bald Mountain batholith. Error ellipses and calculated ages are given at the 95% confidence level. MSWD—mean square of weighted deviates. Dashed error ellipses were excluded in weighted average age calculations.

TABLE 3. SUMMARY OF ZIRCON U-Pb, Lu-Hf, AND O ISOTOPE DATA

Unit	Sample	Pb/U zircon age ± 2SD (Ma) (MSWD; n)	Xenocrystic zircon? (age)	$\delta^{18}\text{O}$ (zircon) average ± 2SD ‰ (n)	$\delta^{18}\text{O}$ (zircon) range (‰)	ϵHf initial (zircon) weight average ± 2SD (MSWD; n)	ϵHf initial (zircon) range
Norite of Badger Butte	BM10-54	156.9 ± 1.4 (0.8; 10)	Yes (ca. 164 Ma)	9.3 ± 0.5 (6)	9.0–9.6	7.0 ± 1.0 (1.8; 11)	4.7–10.6
Quartz diorite of Wolf Creek	BM10-48	>155	No.	9.4 ± 1.0 (7)	8.9–10.0	7.7 ± 1.3 (0.04; 2)	7.5–7.8
Granite of Anthony Butte	BM10-49	154.7 ± 1.3 (1.0; 11)	No	8.5 ± 0.5 (10)	8.2–9.1	7.8 ± 1.4 (4.4; 10)	4.7–10.3
Granodiorite of Anthony Lake	BMO-1	146.7 ± 2.1 (1.3; 11)	No	8.2 ± 0.4 (7)	7.8–8.4	7.6 ± 1.7 (0.1; 17)	6.0–9.6
Tonalite of Bald Mountain	BM10-53	140.9 ± 2.0 (0.5; 7)	Yes (ca. 147–150 Ma)	9.7 ± 0.4 (12)	9.3–10.0	6.5 ± 1.3 (3.7; 12)	3.5–9.8
	BM10-55	141.2 ± 1.9 (1.0; 9)	Yes (ca. 147 Ma)	8.0‰ ± 0.5 (7)	7.7–8.2	7.9 ± 1.3 (4.3; 12)	4.8–10.7
	BM10-51	142.8 ± 1.5 (0.6; 8)	Yes (ca. 146–147 Ma)	7.5 ± 0.5 (8)	7.1–7.8	9.1 ± 1.3 (4.8; 11)	6.5–12.8
	BM10-50	145.1 ± 1.7 (1.5; 24)	Yes (ca. 156 Ma)	n.d.	n.d.	n.d.	n.d.

Note: MSWD—mean square of weighted deviates; SD—standard deviation; n—number; n.d.—no data.

field relationships, we recognize two subgroups that we classify as the type 1 high-Sr/Y tonalite-granodiorite suite and type 2 low Sr/Y tonalite suite.

Type 1 tonalites and granodiorites are typically located south of intraplutonic contact A-B (Fig. 3). They are distinguished from older batholithic rocks and the type 2 tonalite-granodiorite suite by high average Sr/Y values (>40), elevated Sr (>450 ppm, but lower than some older units as stated for the norite-granite rocks), and low Y concentrations (<11.6 ppm; Fig. 6D). They display significant drawdown across the middle REEs and HREEs and lack Eu anomalies (Fig. 7C). They also have lower average HREE (Yb < 1.0 ppm) abundances relative to the type 2 suite (Fig. 7C). Relative to NMORB, they are LILE enriched, have strongly positive Pb and Sr anomalies, and negative Nb anomalies (Fig. 7D). Four whole-rock samples from the tonalite of Bald Mountain yielded $\delta^{18}\text{O}$ values of 9.1‰–12.1‰, and the granodiorite of Anthony Lake yielded a value of 9.6‰. Average zircon and apatite saturation temperatures are 728 °C and 885 °C for the type 1 suite, respectively (Watson and Harrison, 1983; Harrison and Watson, 1984).

Type 2 tonalites occur primarily within the northernmost pluton, north of intraplutonic contact A-B in Figure 3 (e.g., BM10–51). These samples are distinct from the main batholith in having lower Sr/Y (<40), and higher Y (>15 ppm) and total REE concentrations at equivalent SiO_2 concentrations (Figs. 6 and 7). Type 2 samples also have an extended range of SiO_2 concentrations (52–70 wt%) that are some of the lowest values of the batholith. Two whole-rock samples yielded $\delta^{18}\text{O}$ values of 12.7‰–13.1‰. Average zircon and apatite saturation tempera-

tures are 740 °C and 901 °C, respectively, for the type 2 suite (Watson and Harrison, 1983; Harrison and Watson, 1984).

Plagioclase- and hornblende-bearing mafic enclaves are ubiquitous in the type 1 and 2 suites. They are magnesian and metaluminous, but are distinguished from their host rocks by being calc-alkalic to alkalic-calcic in composition, having lower Sr/Y (typically <20), and higher Y and REE concentrations (Figs. 6 and 7C). Mafic enclaves also display low SiO_2 (<60 wt%) concentrations relative to typical host rocks. Relative to NMORB, enclaves are LILE enriched, and have negative Nb and Ti anomalies. Two mafic enclaves from the tonalite of Bald Mountain yielded $\delta^{18}\text{O}$ (WR) values of 8.4‰ and 8.5‰.

Mineral Geochemistry

Plagioclase-Hornblende Geochemistry

We evaluated 14 hornblende-plagioclase pairs from 2 samples from the granodiorite core of the batholith near Anthony Lake for thermobarometry (Supplemental File [see footnote 1]). The average temperature from these coexisting pairs using the Holland and Blundy (1994) plagioclase-hornblende exchange thermometer is 683 ± 41 °C. Pressure is estimated at 0.9 ± 0.6 kbar using the Anderson and Smith (1995) Al-in-hornblende barometer.

Zircon Trace Element Geochemistry

We also investigated the relationship between Pb/U age and zircon trace element chemistry through time (Supplemental File [see footnote 1]). REE abundances are shown in Figure 8 and trace element concentrations are plotted in Figures 9 and 10. Zircons from the type 1 and 2 tonalite-granodiorite suites are distin-

guished from older norite-granite zircons by higher average Hf concentrations and lower U and trivalent cation concentrations (Figs. 9A, 9B). Th/U values from the type 1 and 2 suites are slightly lower, but also overlap with those of zircons from older suites (Fig. 10C). Within the tonalite-granodiorite suite, type 2 zircons from the northernmost tonalite sample (BM10-51) consistently plot as a distinct population, displaying higher average U, Y, and HREE concentrations, and lower Eu/Eu* values versus type 1 zircons. These features are more similar to zircons from the older norite-granite suite.

Zircon Lu-Hf Isotope Geochemistry

Lu-Hf isotopic data were collected from 58 zircons to evaluate possible changes in sources and petrogenetic processes through time (cf. Figs. 9C and 11A; Supplemental File [see footnote 1]). Data from the norite-granite and granodiorite-tonalite suites are summarized in Table 3. Magmatic zircons from the older, low-Sr/Y norite-granite suite yield error-weighted average (2σ), initial ϵHf values ranging from 7.0 to 7.8. Initial ϵHf values for type 1 and 2 zircons of the granodiorite-tonalite suite largely overlap with those from the norite-granite suite, yielding values ranging from 6.5 to 9.1. Average individual sample population errors are ~ 1.3 epsilon units for all samples and are very close to the long-term reproducibility of the standard (FC-1). This suggests that these magmas are fairly well described by these average values. Although there is little statistical difference at the 2σ level in initial ϵHf between the norite-granite and tonalite-granodiorite suites, average $^{176}\text{Lu}/^{177}\text{Hf}$ values decrease from the older to the younger suite (Fig. 10E) regardless of SiO_2 concentration. This trend appears similar

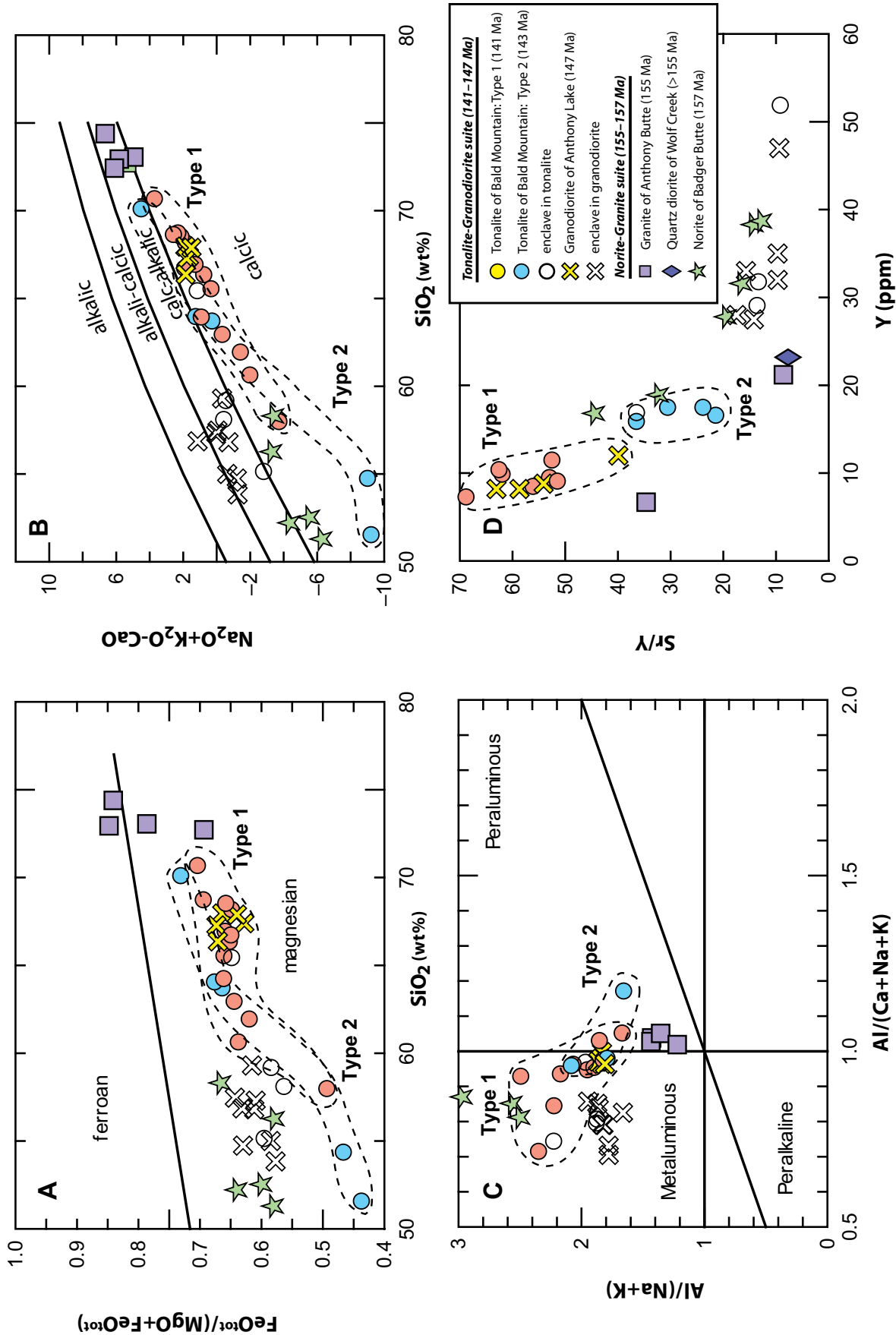


Figure 6. Selected major and trace element plots for plutonic rocks of the Bald Mountain batholith. (A) Fe-number versus SiO_2 illustrating the overall magnesian character of the batholith. (B) Modified alkali lime index (MALI). Mafic enclaves are calc-alkalic, whereas host rocks are calcic. (C) Shand (1947) rock classification index. Batholith rocks are largely metaluminous. (D) Sr/Y versus Y (ppm). Tonalites and granodiorites have high Sr/Y values (>40), whereas rocks of the norite-granite suite have generally lower Sr/Y. Mafic enclaves in type 1 and 2 tonalites and granodiorites overlap in composition and display low Sr/Y values.

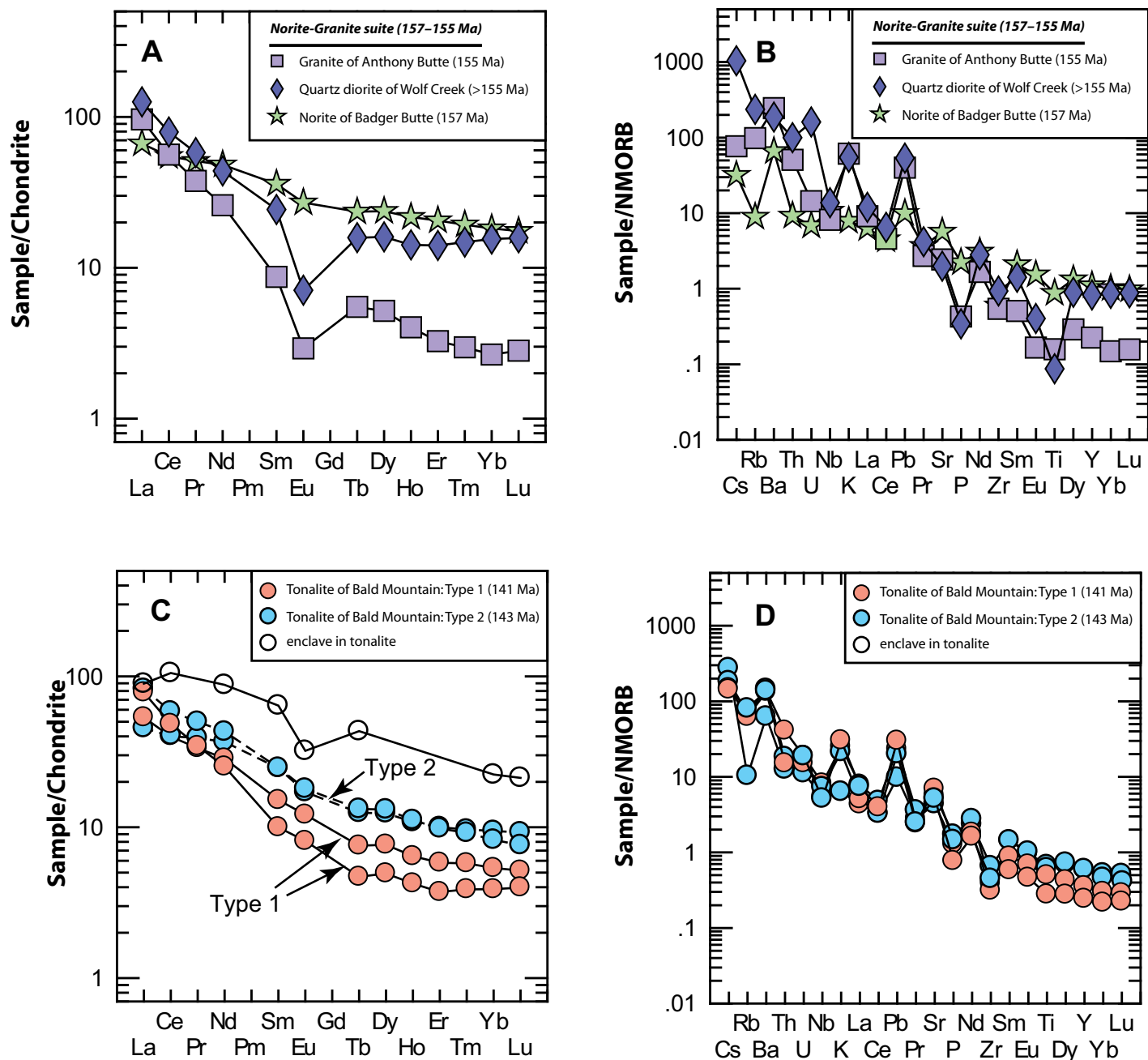


Figure 7. Chondrite-normalized rare earth element (REE) and normal mid-oceanic ridge basalt (NMORB) normalized trace element abundance diagrams for whole-rock samples. (A, B) Chondrite-normalized abundance diagrams for the norite-granite suite. (C, D) Chondrite-normalized abundance diagrams for the tonalite-granodiorite suite including coeval mafic enclaves. Samples are normalized to chondrite and NMORB values of Sun and McDonough (1989). Type 1 tonalites and granodiorites show depletions in heavy REEs relative to type 2 tonalites. Both type 1 and 2 rocks lack deep Eu anomalies that characterize some of the older granites and diorites.

to the pattern of higher average Hf contents and lower HREE concentrations in zircons from the tonalite-granodiorite suite. It is noteworthy that type 2 zircons from the northernmost tonalite sample (BM10-51) overlap, but extend to higher average $^{176}\text{Lu}/^{177}\text{Hf}$ values compared to the more abundant type 1 zircons of the tonalite-granodiorite suite, despite similar SiO_2 contents.

Zircon Oxygen Isotope Geochemistry

We made 59 oxygen isotope measurements on 45 magmatic zircons from the Bald Mountain batholith (Figs. 11B and 12). Rock-average $\delta^{18}\text{O}$ (Zrn) values are summarized in Tables 1 and 3. All individual analyses are provided in the Supplemental File (see footnote 1). Multiple spots were measured on a subset of zircons to

test whether $\delta^{18}\text{O}$ values vary systematically from cores to rims, but we did not observe systematic variations within the analytical precision of the data (cf. Fig. 4).

Cores and rims of magmatic zircon from the norite-granite suite have a mean $\delta^{18}\text{O}$ of $9.3\text{‰} \pm 0.5\text{‰}$ (norite of Badger Butte), $8.5\text{‰} \pm 0.5\text{‰}$ (granite of Anthony Butte), and $9.7\text{‰} \pm 2.0\text{‰}$

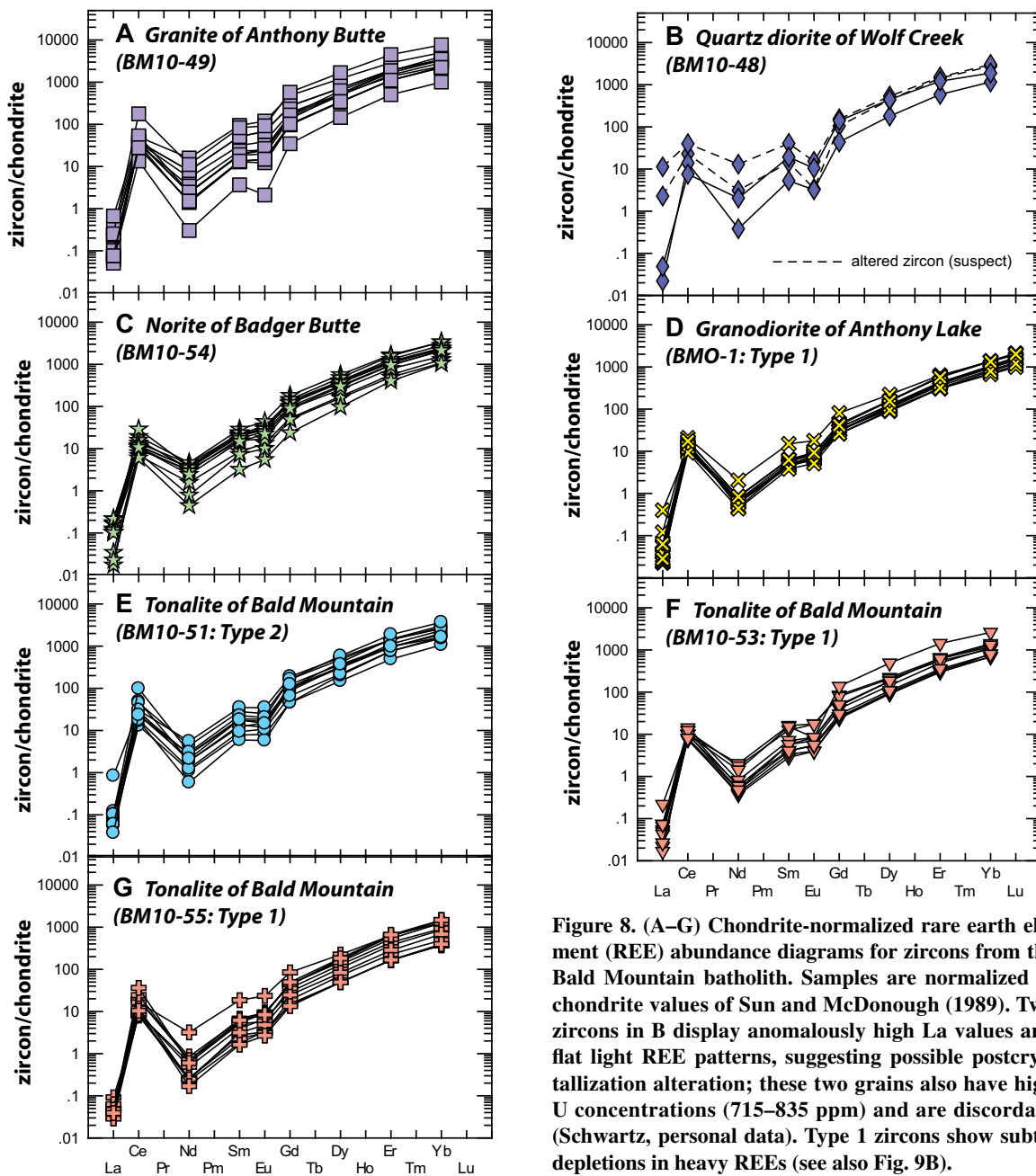


Figure 8. (A–G) Chondrite-normalized rare earth element (REE) abundance diagrams for zircons from the Bald Mountain batholith. Samples are normalized to chondrite values of Sun and McDonough (1989). Two zircons in B display anomalously high La values and flat light REE patterns, suggesting possible postcrystallization alteration; these two grains also have high U concentrations (715–835 ppm) and are discordant (Schwartz, personal data). Type 1 zircons show subtle depletions in heavy REEs (see also Fig. 9B).

(quartz diorite of Wolf Creek). One undated and possibly xenocrystic zircon from the quartz diorite of Wolf Creek yields an anomalous value of 12.0‰. Excluding this analysis gives a mean $\delta^{18}\text{O}$ value of $9.4\text{‰} \pm 1.0\text{‰}$ ($n = 7$).

In general, $\delta^{18}\text{O}$ values for magmatic zircons from the tonalite-granodiorite suite partially overlap with values from the older granite-norite suite, but also extend to lower values (cf. Figs. 11B and 12; Table 3). Type 1 zircons from the granodiorite core of the batholith have a mean $\delta^{18}\text{O}$ value of $8.2\text{‰} \pm 0.4\text{‰}$. Type 1 zircons from the sample near the center of the tonalite

of Bald Mountain (BM10-55 in Fig. 11) have a mean $\delta^{18}\text{O}$ value of $8.2\text{‰} \pm 1.0\text{‰}$. One zircon core gave an anomalously high $\delta^{18}\text{O}$ value of 9.4‰ (Fig. 4). Excluding this value, the mean $\delta^{18}\text{O}$ value of zircons from BM10-55 is $8.0\text{‰} \pm 0.5\text{‰}$. Type 1 zircons from the southernmost sample of the tonalite of Bald Mountain (BM10-53) have a mean $\delta^{18}\text{O}$ value of $9.0\text{‰} \pm 0.4\text{‰}$. Type 2 zircon cores and rims from the northernmost sample of the tonalite of Bald Mountain (BM10-51) have a mean $\delta^{18}\text{O}$ value of $7.5\text{‰} \pm 0.5\text{‰}$. These zircons have the lowest $\delta^{18}\text{O}$ values from the batholith.

DISCUSSION

Timing of Batholith Construction

U-Pb zircon geochronology of the Bald Mountain batholith indicates that magmatic construction occurred over a protracted interval of ~15 m.y. and involved two distinct magmatic episodes involving emplacement of small, low-Sr/Y norites and granites from 157 to 155 Ma, and more areally extensive tonalites and granodiorites from 147 to 141 Ma. Our age determinations from the tonalite-granodiorite suite are consistent with

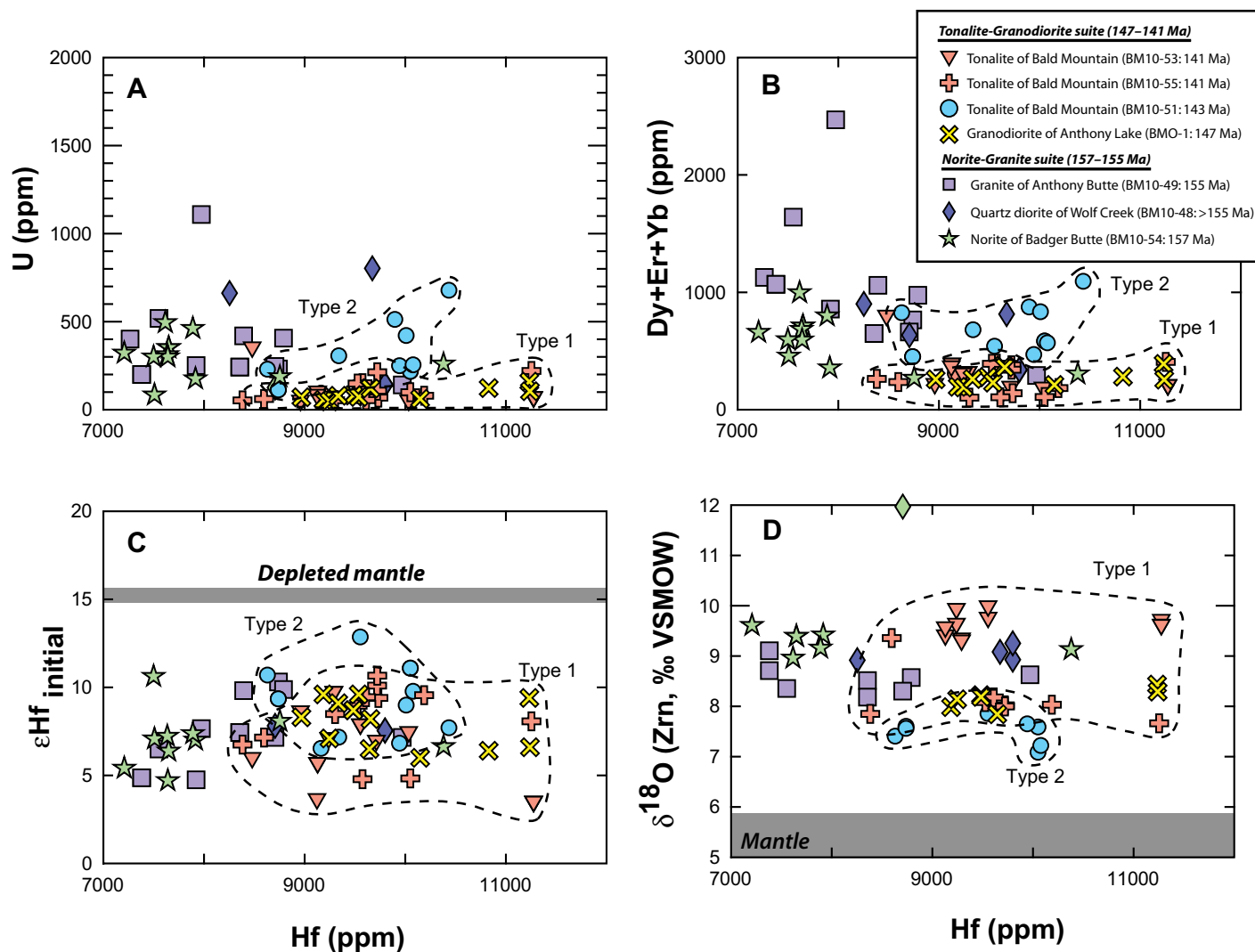


Figure 9. Selected zircon trace element and isotopic values versus Hf (ppm). The low-Sr/Y norite-granite suite is distinguished in part by lower average Hf and higher heavy rare earth element (HREE) concentrations. (A) U versus Hf. (B) HREE (Dy + Er + Yb) versus Hf. (C) Initial ϵ_{Hf} versus Hf. (D) $\delta^{18}\text{O}(\text{Zrn})$ versus Hf. Zircons from the type 1 and 2 tonalite-granodiorite suites are distinguished from older norite-granite zircons by higher average Hf concentrations, and lower U and trivalent cation concentrations. VSMOW—Vienna standard mean ocean water.

the single age from Walker (1989), but also indicate that the pulse of tonalite-granodioritic magmatism was transient and restricted to a 6 m.y. interval. Moreover, our ages also demonstrate that although the low- and high-Sr/Y suites are geographically coincident, they are not temporally or genetically linked. From a regional perspective, the low-Sr/Y suite was emplaced during the final stages of arc-arc collision (159–154 Ma; Schwartz et al., 2011a). The amagmatic interval in the Blue Mountains province lasted for ~6 m.y. and was followed by a renewed phase of regionally extensive, high-Sr/Y magmatism that extended from the Blue Mountains in Oregon to the Klamath Mountains in northern California (Barnes et al., 1996, 2006; Schwartz et al., 2011b).

The primary batholith construction phase commenced with ca. 147 Ma intrusion of the high-Sr/Y granodiorite of Anthony Lake (Schwartz et al., 2011a), which is currently exposed in the core of the batholith. Subsequently, tonalitic magmas intruded the core granodiorite between 145 and 141 Ma, and involved emplacement of three large tonalite bodies (both type 1 and type 2 tonalite suites). Taubeneck (1957, 1995) distinguished these as separate intrusions based on apparent intraplutonic contacts (Fig. 3; A-B and C-D) and mineralogical differences. Within the resolution of our geochronologic data, we cannot distinguish whether these intrusions are distinct in age; however, we note that they are distinct

in geochemistry (see following) and likely represent three separate, large magmatic units that exhibit subtle intraplutonic contacts.

Magma Sources and the Role of Supracrustal Assimilation

Norite-granite plutons in the Bald Mountain batholith are characterized by LREE and LILE enrichment, and weakly positive to negative Nb anomalies. Relative to the main tonalite-granodiorite suite (type 1), rocks from the norite-granite suite display low Sr concentrations (<400 ppm), Sr/Y (<40), and high Y (>15 ppm) values. One sample from the norite of Willow Lake yields a low initial $^{87}\text{Sr}/^{86}\text{Sr}$ (0.7037).

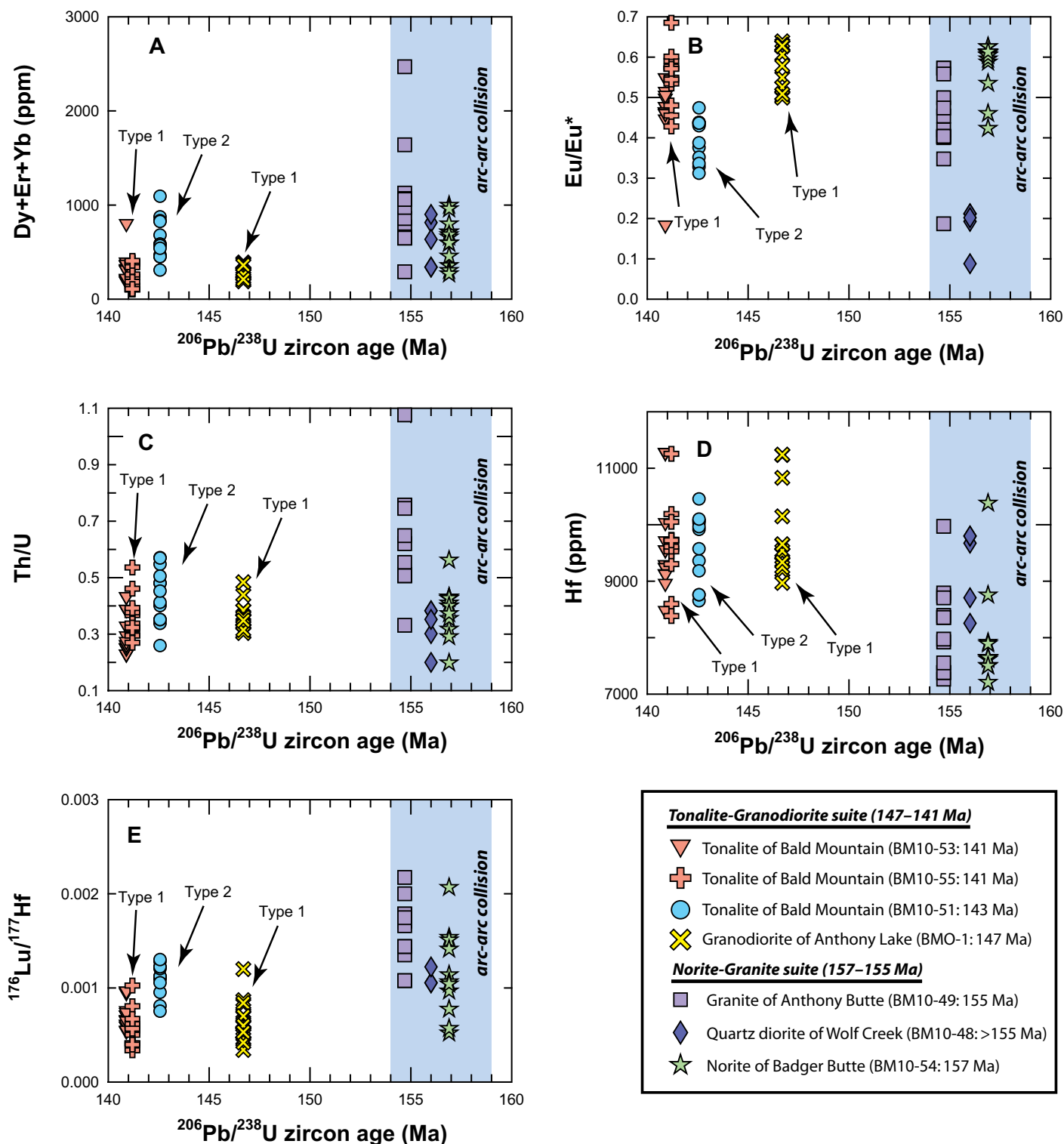


Figure 10. Selected zircon trace element and isotopic values versus $^{206}\text{Pb}/^{238}\text{U}$ age. Timing of arc-arc collision is shown by the blue field (Schwartz et al., 2011a). (A) Heavy rare earth element (HREE) (Dy + Er + Yb) (ppm) versus $^{206}\text{Pb}/^{238}\text{U}$ age. (B) Eu/Eu^* versus $^{206}\text{Pb}/^{238}\text{U}$ age. (C) Th/U versus $^{206}\text{Pb}/^{238}\text{U}$ age. (D) Hf (ppm) versus $^{206}\text{Pb}/^{238}\text{U}$ age. (E) $^{176}\text{Lu}/^{177}\text{Hf}$ versus $^{206}\text{Pb}/^{238}\text{U}$ age. Zircons from postcollisional tonalites and granodiorites show lower concentrations of HREEs, higher Eu/Eu^* values, and lower average Th/U values. They overlap, but also extend to higher Hf concentrations as well.

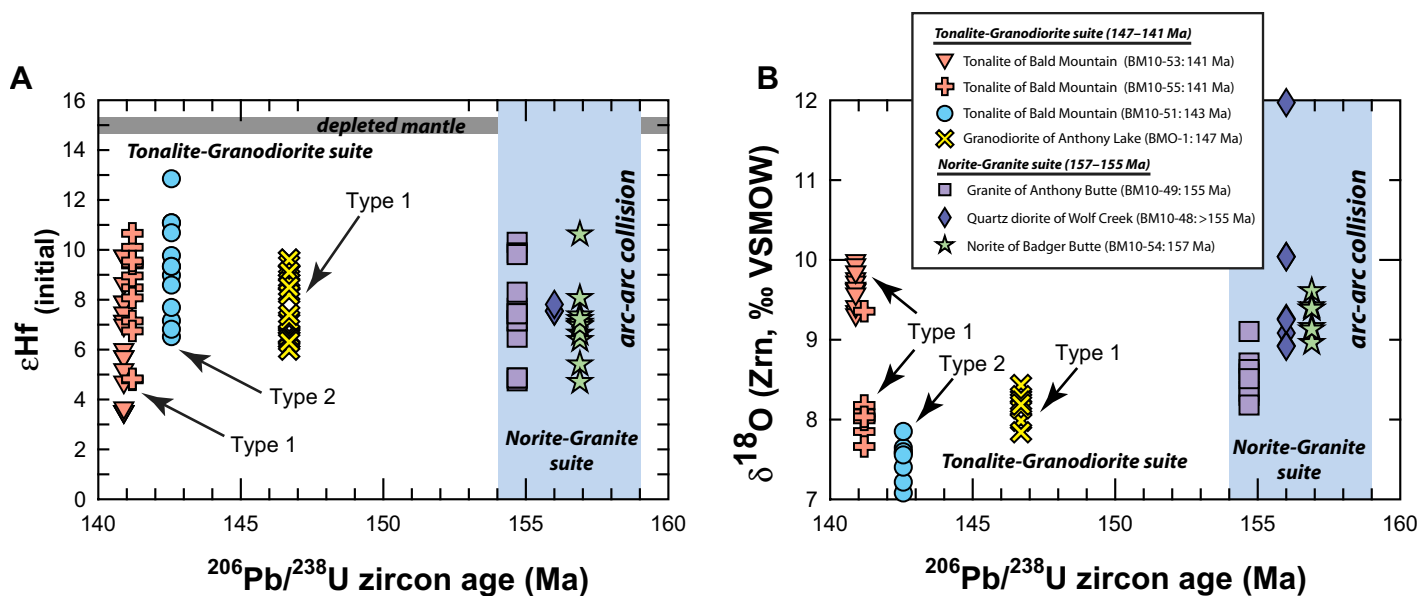


Figure 11. (A) Zircon (initial) ϵHf versus $^{206}\text{Pb}/^{238}\text{U}$ age. (B) $\delta^{18}\text{O}$ (Zrn) versus $^{206}\text{Pb}/^{238}\text{U}$ age. Timing of arc-arc collision is shown by the blue field (Schwartz et al., 2011a). VSMOW—Vienna standard mean ocean water. Symbols as in Figure 10. Both tonalite-granodiorite and norite-granite suites overlap with respect to ϵHf values and $\delta^{18}\text{O}$ (Zrn); however, type 2 zircons from the northern tonalite pluton extend to lower $\delta^{18}\text{O}$, suggesting less interaction with supracrustal rocks.

Apatite saturation temperatures for the norite-granite suite range from ~ 770 to 900 °C. These features are collectively similar to those found in magmas generated in oceanic island-arc settings and are indicative of hydrous partial melting of mantle peridotite and/or mafic-arc crust (Kelemen et al., 2003).

Although whole-rock trace element geochemical features discussed here suggest a mantle and/or mafic-arc crust source for these rocks, oxygen and Hf isotopic compositions of zircons also provide evidence for supracrustal contamination. For example, initial ϵHf values are moderately positive (+6.3–7.9), yet they are substantially lower than depleted mantle ca. 147 Ma (~ 15 ; Vervoort et al., 1999) and average modern island-arc values (~ 13 ; Dhuime et al., 2011; cf. Fig. 11A). Similarly, $\delta^{18}\text{O}$ (Zrn) values (8.2‰–10.0‰) are much higher than values in high-temperature equilibrium with the mantle ($5.3\text{‰} \pm 0.6\text{‰}$; Valley, 2003) and indicate significant incorporation of a high- $\delta^{18}\text{O}$ component (Fig. 11B). Field observations indicate that both the Badger Butte norite and the Anthony Butte granite intrude the Elkhorn Ridge Argillite, which has high $\delta^{18}\text{O}$ (WR) values ranging from 22.0‰ to 27.6‰, radiogenic $^{87}\text{Sr}/^{86}\text{Sr}$ values of 0.7113–0.7128, and negative ϵNd values of -6.9 to -10.0 at 147 Ma. The Anthony Butte granite in particular contains large xenoliths of country rock, which compose as much as 20 vol% of the intrusion overall (Taubeneck, 1995). Small degrees of assimilation of high $\delta^{18}\text{O}$ Elkhorn Ridge Argillite may explain the high $\delta^{18}\text{O}$ (WR)

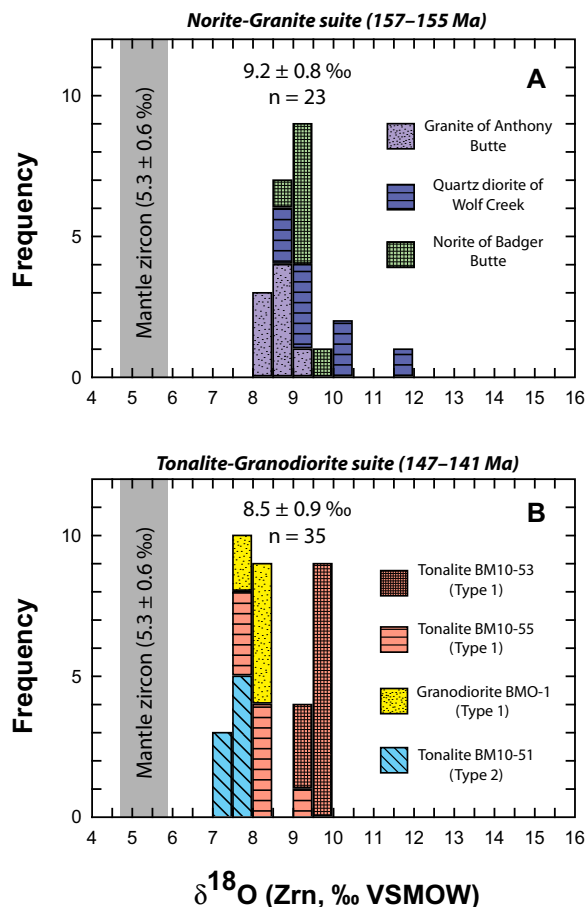
values in the norite-granite suite and would not significantly change whole-rock major element compositions.

Assimilation of high $\delta^{18}\text{O}$ Elkhorn Ridge Argillite would not only change oxygen and Hf isotopes, but would also change the whole-rock major and trace element composition of the parental magma. We test the validity of argillite assimilation by assuming a 3‰ increase in $\delta^{18}\text{O}$ (WR) values from $\sim 7\text{‰}$ – 10‰ by bulk assimilation of average Elkhorn Ridge Argillite with a value of +25‰. With these parameters, bulk mass balance calculations suggest $\sim 15\%$ assimilation and/or exchange of Elkhorn Ridge Argillite oxygen. Using the compositions of a norite (BM10-54) and Elkhorn Ridge Argillite (DB-06–34; Supplemental File [see footnote 1]), whole-rock mass balance calculations yield realistic basaltic parental (pre-assimilation) magma compositions with the following values: SiO_2 , 47.6 wt%; Al_2O_3 , 19.5 wt%; CaO , 11.6 wt%; $\text{FeO}^{\text{total}}$, 9.4 wt%; MgO , 6.8 wt%; Sr , 550 ppm; Ba , 378 ppm. The Elkhorn Ridge Argillite is characterized by low Al_2O_3 concentrations (typically < 15.5 wt%), which are similar to or less than all plutonic rocks in the Bald Mountain batholith. Consequently, assimilation of Elkhorn Ridge Argillite has a modest effect on the major element (e.g., Al_2O_3) and trace element compositions and yields values consistent with a high Al-basaltic primary magma composition (see hypothetical calculated compositions herein). Compositions similar to those predicted here are also found in the norite of Badger Butte

(e.g., BMB-10) and in the nearby North Fork pluton (Johnson and Schwartz, our data).

Tonalites and granodiorites from the type 1 suite have major and trace element characteristics similar to melts produced by dehydration–partial melting of garnet-bearing basaltic sources such as garnet amphibolite and/or eclogite at high pressures (> 1.0 Gpa; e.g., Wolf and Wyllie, 1993, 1994; Rapp, 1995). For example, type 1 tonalites and granodiorites have low Mg numbers (~ 40 – 50) and high Al_2O_3 concentrations (> 15 wt%) that overlap the range of experimental melts produced by dehydration–partial melting of amphibolites (Sen and Dunn, 1994; Rapp and Watson, 1995). Type 1 tonalites and granodiorites also display low HREE (Yb < 1.0 ppm) and Y (< 11.6 ppm) abundances, high LREE/HREE ($\text{La}/\text{Yb} > 13.9$), high Sr abundances (> 450 ppm), and high Sr/Y values (> 40). Elevated Sr contents (> 400 ppm) and a lack of Eu anomalies in whole rock, chondrite-normalized REE abundance patterns further suggest that plagioclase was not a residual phase in the restite or a prominent crystal fractionate. The lack of positive Eu anomalies, and Al_2O_3 and CaO concentrations < 20 wt% and 10 wt%, respectively, also indicate that type 1 tonalites and granodiorites have not undergone significant crystal accumulation. Relatively low initial $^{87}\text{Sr}/^{86}\text{Sr}$ values of 0.7038–0.7044 are indicative of juvenile mafic crust as a potential source for members of the tonalite-granodiorite suite. These magma compositions are similar to hydrous melts produced by dehydration melting

Figure 12. (A) Histogram of $\delta^{18}\text{O}$ (Zrn) for low-Sr/Y, norite-granite suite. (B) Histogram of $\delta^{18}\text{O}$ (Zrn) for high-Sr/Y, tonalite-granodiorite suite. Both suites are characterized by elevated $\delta^{18}\text{O}$ values relative to the mantle; however, the tonalite-granodiorite suite extends to slightly lower $\delta^{18}\text{O}$ values. Mantle-equilibrated zircon value of 5.3 ± 0.6 ‰ (2 standard deviation) is from Valley (2003). VSMOW—Vienna standard mean ocean water.



experiments in which the residuum consists of a plagioclase-poor to absent, garnet + amphibole + clinopyroxene ultramafic assemblage. Such assemblages are common in granulite terranes that have undergone dehydration–partial melting of mafic sources (e.g., lower crust of Kohistan; Garrido et al., 2006), and garnet amphibolites occur within the Blue Mountains province in the Salmon River suture zone (Selverstone et al., 1992) and the Mine Ridge area of the Greenhorn subterrane of the Baker terrane (Hooper et al., 1995).

Zircons from the type 1 suite display initial ϵ_{Hf} values ranging from 6.3 to 8.9 and elevated $\delta^{18}\text{O}$ values of 7.1‰–10.0‰ (Figs. 11A, 11B). These high $\delta^{18}\text{O}$ zircon values are similar to values reported from peraluminous magmas derived from partial melting and/or assimilation of supracrustal rocks (e.g., King and Valley, 2001; Lackey et al., 2006, 2008; Kemp et al., 2007; Appleby et al., 2010), and suggest considerable mixing or exchange with a high $\delta^{18}\text{O}$ component. In the Sierra Nevada batholith, metaluminous to peraluminous plutons with elevated $\delta^{18}\text{O}$ values and low initial $^{87}\text{Sr}/^{86}\text{Sr}$ values have been interpreted to be derived in large part from recycling of hydrothermally altered (high $\delta^{18}\text{O}$)

oceanic crust and/or relatively young volcanogenic sedimentary rocks (Lackey et al., 2006). A possible origin for the high $\delta^{18}\text{O}$ magmas of the Bald Mountain batholith may include partial assimilation of hydrothermally altered mafic arc crust (e.g., Wallowa-derived metagabbros) or supracrustal metasedimentary rocks (e.g., Elkhorn Ridge Argillite), both of which occur as xenoliths within the tonalite-granodiorite suite. Although partial assimilation from both sources is possible, field evidence reveals minor reaction textures and little to no migmatization of foliated metagabbro xenoliths (Taubeneck, 1995). In contrast, partial assimilation of Elkhorn Ridge Argillite is more likely on the basis of field observations, including (1) reaction halos surrounding cherty argillite xenoliths in tonalite and granodiorite, and (2) the abundance of cherty argillite in wall rocks of the contact aureole, and their conspicuous scarcity among xenoliths within the batholith. Equilibrium phase diagram (pseudosection) modeling of the Elkhorn Ridge Argillite (ERA-1 in the Supplemental File [see footnote 1]) also predicts low solidus temperatures (650–675 °C at 1.5–7.5 kbar), indicating that assimilation was likely during magma evolution either at depth, or at the current level of

emplacement. Assimilation of radiogenic Elkhorn Ridge Argillite ($^{87}\text{Sr}/^{86}\text{Sr} = 0.7113\text{--}0.7128$) is also supported by elevated, non-mantle $\delta^{18}\text{O}$ (Zrn) values and enrichment in initial $^{87}\text{Sr}/^{86}\text{Sr}$ of the tonalite-granodiorite (0.7038–0.7044) suite relative to metagabbros (0.7032–0.7036). Isotopic mass balance calculations using average initial $^{87}\text{Sr}/^{86}\text{Sr}$ of the tonalite-granodiorite suite and average Elkhorn Ridge Argillite yield ~20% bulk mixing with Elkhorn Ridge Argillite. Some mixing could have occurred at depth; this is a likely scenario given that the Bald Mountain batholith was emplaced into a major terrane boundary between the Baker terrane and arc-related rocks of the Wallowa terrane. In the following section, we explore various magma evolution scenarios through whole-rock and zircon geochemical modeling.

Mafic enclaves are a ubiquitous feature in the type 1 and type 2 tonalite-granodiorite suites and contain information about the nature of magma sources and magma mixing and/or recharge during batholith construction. Field observations indicate that some dioritic enclaves display fine-grained chilled margins against host granodiorites, suggesting that they are coeval magmas. Mafic enclaves are distinct from host rocks in being calc-alkalic to alkalic-calcic, having much higher Y and HREE concentrations (cf. Figs. 6 and 7), and having lower Sr/Y values (<40) at equivalent Mg# (Fig. 13C). Mafic enclaves also have lower $\delta^{18}\text{O}$ values (WR = 8.4‰–8.5‰) than measured $\delta^{18}\text{O}$ (WR) values for host tonalites and granodiorites (9.6‰–13.1‰). However, $\delta^{18}\text{O}$ values of enclaves are still greater than expected for basaltic melts in equilibrium with mantle (Harrison and Hoefs, 1995), which is also consistent with minor assimilation of Elkhorn Ridge Argillite by the parental magma of the enclaves. The LILE enrichment and negative Nb and Ti anomalies suggest that the enclaves formed from subduction-related partial melting of mantle peridotite. These characteristics indicate that enclaves represent a distinct and unrelated magma to those that formed the tonalite-granodiorite suite. Further, the presence of mafic enclaves may indicate the presence of larger volumes of mafic magma at depth and would provide a heat source for partial melting of lower arc crust (see partial melting models discussion following).

Type 2 tonalites occur in the northernmost augite-hornblende pluton and are geochemically similar to low-Sr/Y mafic enclaves. They are both characterized by low average Sr/Y values (<40), and higher Y (>16 ppm) and HREE (Yb > 1.3 ppm) concentrations. Similarly, type 2 zircons are characterized by higher average U, Y, and HREE concentrations, and lower Eu/Eu* values relative to type 1 zircons (Figs.

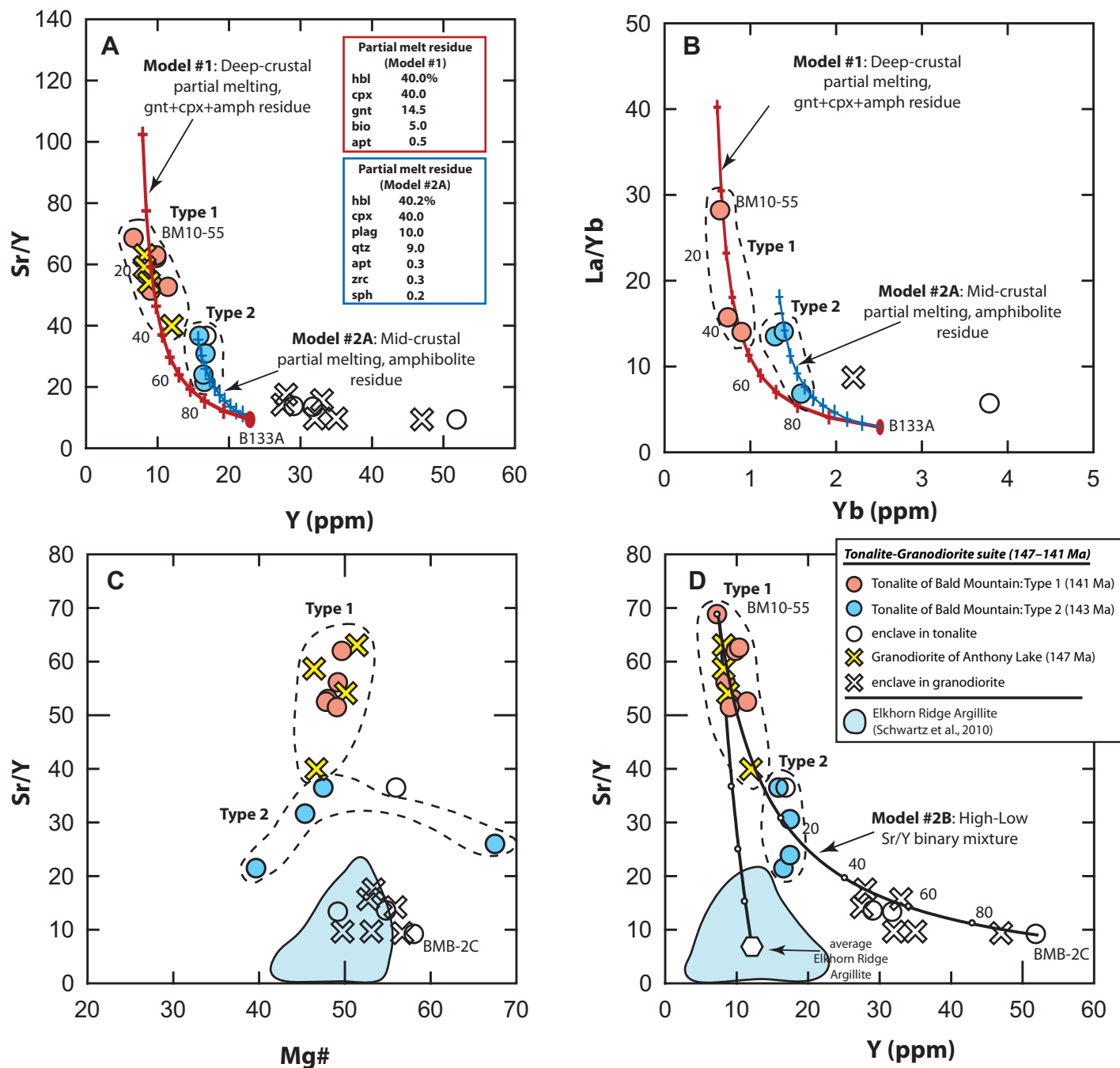


Figure 13. (A, B) Results of partial melting calculations with a metagabbro source rock (B133A). Partial melting results in the generation of an amphibole + clinopyroxene (cpx) + garnet (gnt) restite. Abbreviation: hbl—hornblende, cpx—clinopyroxene, bio—biotite, apt—apatite, plag—plagioclase, qtz—quartz, zrc—zircon, sph—sphene, amph—amphibole. The partial melting curve describes the majority of the data and predicts a melt fraction between 10% and 40% for most samples. Several type 2 tonalite samples with low Sr/Y values (<40) are not well described by the partial melting curve and yield unrealistically large melt fractions (50%–80%). Binary mixture models (e.g., Fig. 13D) suggest that they may be mixtures of high- and low-Sr/Y magmas. (C) Sr/Y versus Mg#. Samples from the tonalite-granodiorite suite display decreasing Sr/Y values with decreasing Mg#, consistent with a plagioclase fractionation trend. Mafic enclaves are distinct from host tonalite-granodiorite with distinctly low Sr/Y at equivalent Mg#. Mg# is calculated as $100 \times \text{molar MgO}/(\text{MgO} + \text{FeO}^{\text{tot}})$. (D) Results of binary mixture models between a high-Sr/Y tonalite end member and (1) a low-Sr/Y mafic enclave and (2) average Elkhorn Ridge Argillite. The binary mixture model involving high and low-Sr/Y magmas fairly accurately describes the composition of the low-Sr/Y type 2 tonalites from the northernmost pluton. Sample numbers are listed in Table 1.

9–10). Values of $\delta^{18}\text{O}$ (Zrn) in the northernmost pluton range from 7.1‰ to 7.8‰ and are the lowest recorded from the tonalite-granodiorite suite. In contrast to the overall high-Sr/Y nature of the type 1 tonalite-granodiorite suite, the type 2 tonalite suite is geochemically and geographically distinct, and may have a separate, distinct source.

Whole-Rock and Zircon Geochemical Modeling of Type 1 and 2 Tonalite-Granodiorite Magmas

Magmas with high Sr/Y can be generated in a variety of ways including (1) high-pressure partial melting of mafic crust (e.g., Drummond and Defant 1990; Barnes et al., 1996; Petford and Atherton 1996; Johnson et al., 1997), (2) high-pressure fractional crystallization (Arth et al., 1978; MacPherson et al., 2006; Alonso-Perez et al., 2009), and (3) magma mixing (Guo et al., 2007a, 2007b). Here we evaluate the origin of the high-Sr/Y, type 1 tonalites and granodiorites in the Bald Mountain batholith by investigating various fractional crystallization, partial melting, magma mixing, and energy-constrained, recharge-assimilation-fractional crystallization models. We also investigate the origin of the less abundant type 2 low-Sr/Y tonalitic magmas as products of either low-pressure partial melting of mafic crust and/or magma mixing between basaltic melts and high-Sr/Y, type 1 magmas.

Fractional Crystallization Models

Major element mass balance calculations (Bryan et al., 1969) were performed to test whether type 1 and 2 magmas could be generated by fractional crystallization of a common mafic magma. In the case of the high-Sr/Y, type 1 magmas, we use the composition of two primitive low-Sr/Y mafic enclaves (BMB-2C, BMi2) as a parental composition, and the composition of a type 1 high-Sr/Y granodiorite (BMB-4A) as a daughter composition. Although garnet and clinopyroxene are not present in type 1 tonalite-granodiorite suites or in the mafic enclaves, we use values reported in Alonso-Perez et al. (2009) for our models to test whether extraction or retention of garnet + clinopyroxene at depth may have played a role in the generation of the type 1 suite. We also evaluate the role of omphacite as a possible fractionating phase because it is observed together with garnet in the deep roots of some magmatic arcs (e.g., Fiordland, New Zealand; De Paoli et al., 2009). Models were considered successful if the sum of the square of the residuals (ssr) was <1.0, indicating low variation between the calculated and observed daughter compositions. In these calculations we assume perfect Rayleigh fractionation and that

plutonic rocks represent liquid compositions. Trace element and REE fractionation models use partition coefficients reported in Schwartz et al. (2011b) for consistency.

Results from our calculations demonstrate that low-pressure, fractionation of plagioclase + hornblende yield unacceptable results (ssr > 1); however, mass balance calculations involving assemblages fractionating at high pressure, including plagioclase + garnet ± clinopyroxene ± omphacite ± hornblende ± biotite ± sphene ± apatite, were successful (models 5A, 8A, 9A, 11A, 12A, 15A, 17A; Supplemental File [see footnote 1]). These assemblages were further tested with trace element and REE calculations. Whereas several models matched the Sr/Y variations observed in our sample suite, all models failed to reproduce Y and REE concentrations for the type 1 high-Sr/Y tonalite-granodiorite rocks. Fractionation of plagioclase predicted by the high-pressure assemblage is also inconsistent with the high Sr concentrations and absence of Eu anomalies in the tonalite-granodiorite suite. No acceptable solutions were obtained for plagioclase-free, high-pressure fractionation assemblages containing garnet ± clinopyroxene ± omphacite ± hornblende. We conclude, therefore, that fractional crystallization of a low-Sr/Y mafic magma did not produce the type 1 high-Sr/Y magmas in the Bald Mountain batholith.

For type 2 low-Sr/Y magmas, we use the composition of the same two primitive low-Sr/Y mafic enclaves (BMB-2C, BMi2) as a parental composition, and the composition of a type 2 low-Sr/Y tonalite (BM10-51) as a daughter composition. Results from these calculations indicate that fractionation of a plagioclase + hornblende + biotite assemblage with trace (<1 wt%) apatite, sphene, and garnet yields acceptable results (ssr < 1). Acceptable models also reproduced Sr/Y variations for the type 2 suite and yielded similar REE concentrations. These results demonstrate that low-pressure fractional crystallization can account for the geochemical diversity of the type 2 suite.

Partial Melting Models

Major element mass balance (Bryan et al., 1969) and batch partial melting calculations were performed to test whether partial melting of existing mafic arc rocks at depth could have produced the type 1 and 2 magmas. We use the compositions of nearby Triassic mafic arc rocks as our source material for major and trace element calculations (e.g., B133A; Ferns and Brooks, 1995; VS3-1; Vallier, 1995) because they represent Wallowa arc crust that was underthrust beneath the Baker terrane during Late Jurassic collision at 159–154 Ma (Schwartz et al., 2011a). For the type 1 high-

Sr/Y suite, major element mass balance models yielded acceptable results (ssr < 1) for high-pressure mineral assemblages containing omphacite + garnet ± sphene (models 8A, 10A; Supplemental File [see footnote 1]) and low-pressure assemblages containing plagioclase + clinopyroxene ± hornblende ± garnet ± apatite (models 1A, 2A, 3A, and 4A; Supplemental File [see footnote 1]). For the type 2 low-Sr/Y suite, major element mass balance models yielded acceptable results for low-pressure residual assemblages containing plagioclase + clinopyroxene ± hornblende ± sphene ± apatite (models 11A, 12A, 14A, and 15A; Supplemental File [see footnote 1]).

Results from major element mass balance models were evaluated using best-fit partial melting models. Using the same sources, high-pressure assemblages reasonably reproduce the variability in the type 1 high-Sr/Y suite (20%–40% partial melting in model 1; Figs. 13A, 13B); however, the low-pressure fractionation assemblages are not consistent with any predicted partial melting models. This conclusion is consistent with the absence of Eu anomalies and the high Na_2O and Sr concentrations of the tonalite-granodiorite suite that suggest that plagioclase was not a stable residual phase. The calculated restite mineralogy is similar to the observed mineralogy of metagabbros in the Blue Mountains province (Selverstone et al., 1992; Hooper et al., 1995), and agrees well with experimental studies of deep-crustal partial melting of basaltic compositions with garnet as a stable residual phase (Rapp et al., 1991; Rushmer, 1991; Winther and Newton, 1991; Wolf and Wyllie, 1993, 1994).

For the low-Sr/Y, type 2 suite, best-fit partial-melting calculations reproduce the observed geochemical variability with ~10%–40% partial melting and a residual assemblage containing hornblende + clinopyroxene + plagioclase + quartz + trace apatite, zircon and sphene (model 2A in Figs. 13A, 13B). These results indicate that polybaric partial melting of a mafic source rock, such as metagabbros from the underthrust Wallowa island-arc terrane, is capable of producing the variation in trace element compositions observed in type 1 and 2 tonalite-granodiorites in the Bald Mountain batholith.

Magma Mixing Models

Another possibility for the origin of the type 2 magmas is that they are derived from mixing between high-Sr/Y and low-Sr/Y magma (e.g., type 1 magma and mafic enclaves). We constructed simple binary mixture models (Langmuir, 1989) and used a type 1 high-Sr/Y tonalite (BM10-55) and mixed it with a low-Sr/Y, mafic enclave (BMB-2C), and average Elkhorn Ridge Argillite (Fig. 13D). The resulting models for

the type 1 high-Sr/Y magma and mafic enclave demonstrate that 15%–25% mixing of mafic enclave with type 1 magma reproduces the composition of type 2 lower Sr/Y tonalites from the northern portion of the batholith (model 2B in Fig. 13D). Binary mixing models using major elements (e.g., SiO₂, Al₂O₃, CaO, Na₂O, K₂O) and the same type 1 tonalite and mafic enclave end members yield similar results, although in some cases the mixing does not reproduce the composition of sample BM10-50 (e.g., mixture model for Sr/Y versus SiO₂, not shown). In contrast, simple binary mixing of average Elkhorn Ridge Argillite with a high-Sr/Y magma does not satisfactorily reproduce the composition of the low-Sr/Y tonalites (Fig. 13D). These results suggest that the composition of the type 2 lower Sr/Y (<40) tonalites could result from mixing between a type 1 high-Sr/Y magma and a coeval, low-Sr/Y mafic magma. These results are also in agreement with the overall more mafic composition of the type 2 magmas (including the presence of augite as a phenocryst phase), and their lower δ¹⁸O (Zrn) values compared to the type 1 tonalite-granodiorite suite. A problem with this model is that coeval mafic magmas are only present as enclaves and are nowhere found as separate physical entities (e.g., gabbro plutons). Where gabbros and norites are found, they are older (e.g., Badger Butte norite) and are geochemically unrelated. It is possible that enclaves were derived from more extensive basaltic magmas at depth, which are not exposed at the current level of erosion.

Energy-Constrained, Recharge–Assimilation–Fractional Crystallization Models

More complex and realistic models involving energy-constrained, recharge–assimilation–

fractional crystallization (EC-RAFC) were developed to test magma evolution of the high-Sr/Y magmas. We use both whole-rock and zircon trace element and isotopic data and the Spera and Bohron (2002) EC-RAFC model to explore various scenarios. Input parameters for our models are given in Table 4. The εHf values for the assimilant (Elkhorn Ridge Argillite) were calculated from average εNd values reported in Schwartz et al. (2010) using the Verwoort et al. (1999) crustal Hf–Nd relationship; the latter is an empirical best-fit, linear relationship between Hf and Nd isotopes derived from a global study of sediments, continental basalts, granitoids, and juvenile crustal rocks. Although at the fine scale it is likely that Nd and Hf are decoupled, our calculated Hf isotopic values simply serve to approximate the isotopic composition of the Elkhorn Ridge Argillite as an end-member composition. Initial ⁸⁷Sr/⁸⁶Sr values for wall rocks were calculated to 147 Ma from data in Schwartz et al. (2010). Liquidus temperatures for tonalite and recharge magmas were calculated from whole-rock compositions using the MELTS algorithm (Ghiorso and Sack, 1995).

Figures 14A and 14B depict the geochemical evolution of the type 1 tonalite-granodiorite magma as it follows our modeled EC-RAFC path. As temperature decreases from an initial ~1050 °C, the Sr concentration of the magma decreases by fractional crystallization, during which time the wall rock (Elkhorn Ridge Argillite) gradually thermally equilibrates with the magma. When the magma reaches ~675 ppm Sr (or ~890 °C), the wall rock is heated above its solidus and anatectic melts form and are added to the magma, with the net result of increasing the ⁸⁷Sr/⁸⁶Sr and δ¹⁸O values of the magma. Meta-

morphic chlorite and white micas in the Elkhorn Ridge Argillite are likely the first mineral phases to dehydrate. Recharge and homogenization of mantle-derived, low-Sr/Y mafic magmas with the high-Sr/Y magma occurs incrementally throughout the assimilation–fractional crystallization process until complete crystallization at ~200 ppm Sr.

In general, the whole-rock geochemical models fairly accurately reproduce the trends we observe in our data; however, in our Sr versus ⁸⁷Sr/⁸⁶Sr model (Fig. 14A), four data points are below the best-fit magma evolution line suggesting that a lower ⁸⁷Sr/⁸⁶Sr value for the assimilants may be more appropriate for those samples. We also observe slightly more scatter in our measured whole-rock Sr–δ¹⁸O(WR) model (Fig. 14B), which may reflect some degree of low-temperature alteration of whole-rock oxygen isotopes by hydrothermal fluids associated with Tertiary volcanism in the region (Ferns and Taubeneck, 1994).

Intracrystalline diffusion in zircon is very slow for oxygen and Hf, and isotope ratios will not be affected by low-temperature alteration in the absence of radiation damage and a fluid phase (cf. Cherniak et al., 1997; Cherniak and Watson, 2003; Page et al., 2007; Bowman et al., 2011). Thus, analyses of zircons allow us to investigate EC-RAFC models at the mineral scale. Using the same thermal parameters as in the whole-rock models (cf. Table 4), EC-RAFC models also reproduce the variation in our zircon Hf–O data (Fig. 15). We find that slight variations in the Hf concentration of the assimilant from 0.8 to 1.2 ppm encompass the majority of the natural sample variation. Since the Hf budget of the assimilant will largely be contained within detrital zircon, incomplete or partial

TABLE 4. EC-RAFC PARAMETERS FOR Sr–O–Hf GEOCHEMICAL MODELS

Thermal parameters			
Magma liquidus temperature	1050 °C	Crystallization enthalpy of magma (J/kg)	396000
Magma initial temperature (T _{mo})	1050 °C	Isobaric specific heat of magma (J/kg per K)	1484
Assimilant liquidus temperature	800 °C	Fusion enthalpy (J/kg)	270000
Assimilant initial temperature	400 °C	Isobaric specific heat of assimilant (J/kg per K)	1370
Solidus temperature	650 °C	Crystallization enthalpy of recharge magma (J/kg)	396000
Recharge magma liquidus temperature	1150 °C	Isobaric specific heat of recharge magma (J/kg per K)	1484
Recharge magma initial temperature (T _{mo})	1150 °C		
Equilibration temperature (T _{eq})	800 °C		
Compositional parameters			
Magma initial concentration	Sr 800 ppm	δ ¹⁸ O	Hf 1.4 ppm
Magma isotope ratio	0.7045	5.3	15
Magma trace element distribution coefficient	1.5		0.2
Enthalpy of trace element distribution reaction	–		–
Assimilant initial concentration	75 ppm		0.8–1.2 ppm
Assimilant isotope ratio	0.7130	25	–12
Assimilant trace element distribution coefficient	0.05		0.2
Enthalpy of trace element distribution reaction	–		–
Recharge magma initial concentration	600 ppm		2.0 ppm
Recharge magma isotope ratio	0.7035	5.3	15
Recharge magma trace element distribution coefficient	1.5		0.2
Enthalpy of trace element distribution reaction	–		–

Note: EC-RAFC—energy-constrained, recharge–assimilation–fractional crystallization. Dashes indicate no input data.

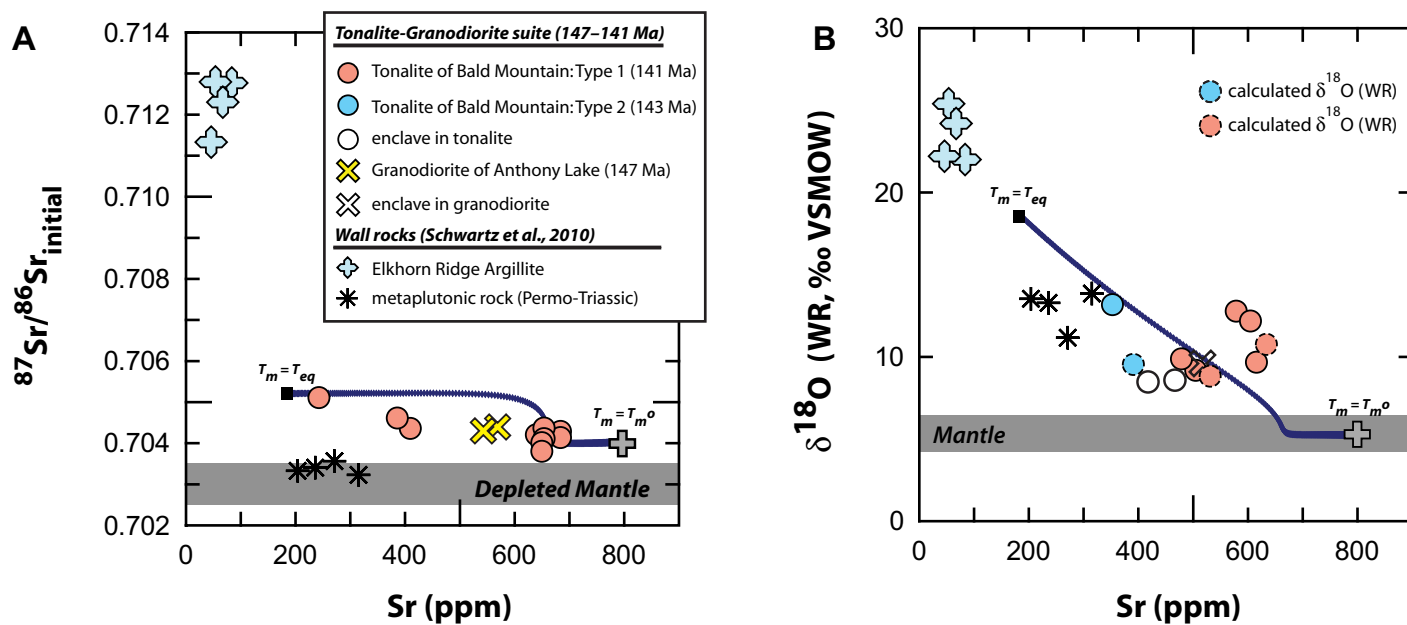


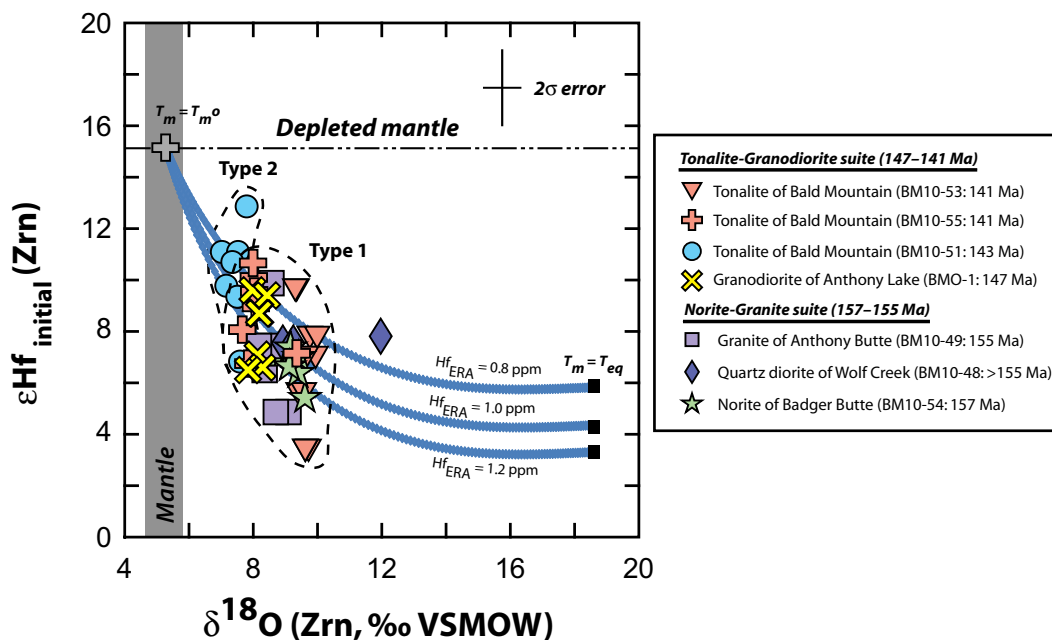
Figure 14. Results of energy-constrained, recharge–assimilation–fractional crystallization (EC-RAFC) models. (A) Initial $^{87}\text{Sr}/^{86}\text{Sr}$ versus Sr for whole-rock samples (data from Armstrong et al., 1977). (B) Measured and calculated $\delta^{18}\text{O}$ (WR—whole rock) versus Sr. VSMOW—Vienna standard mean ocean water. Calculated $\delta^{18}\text{O}$ (WR) were determined from $\delta^{18}\text{O}$ (Zrn) values using the Lackey et al. (2008) equation. Data for Elkhorn Ridge Argillite and metagneous wall rocks are from Schwartz et al. (2010) and Schwartz and Johnson (our data). T_{eq} , T_m , and T_m^0 refer to temperature of equilibration (or final magma temperature in the model), magma temperature, and initial magma temperature, respectively. Parameters for EC-RAFC are provided in Table 4.

dissolution of zircons into the magma prior to zircon saturation could account for the varying Hf concentrations of the assimilant required to describe the data. Detrital zircon cores were not directly targeted for analysis in this study; however, cathodoluminescence imaging reveals

that distinct cores are present as minor components in zircons in most plutonic rocks of the batholith, indicating that incomplete dissolution of preexisting zircon was a likely process during magmatic evolution. Although the EC-RAFC models simulate magma evolution after

emplacement, we note that assimilation of wall rock may also occur at depth during magma ascent. Thus, results of the whole-rock and zircon models underscore the importance of supracrustal (wall rock) contamination in the evolution of the Bald Mountain batholith.

Figure 15. ϵHf (Zrn) versus $\delta^{18}\text{O}$ (Zrn) with results of energy-constrained, recharge–assimilation–fractional crystallization (EC-RAFC) models for the high and low-Sr/Y suites. VSMOW—Vienna standard mean ocean water; ϵHf and $\delta^{18}\text{O}$ mantle zircon compositions are after Vervoort et al. (1999) and Valley (2003). The variation in O and Hf isotope ratios can be reproduced by slight variations in the Hf concentration of the assimilant (ERA—Elkhorn Ridge Argillite). See text for details of the model. T_{eq} , T_m , and T_m^0 refer to temperature of equilibration, magma temperature, and initial magma temperature, respectively. Parameters for EC-RAFC are provided in Table 4.



High-Sr/Y Magmas as Recycled Continental Crust

Geochemical modeling indicates that the type 1 high-Sr/Y magmas are largely derived from partial melting of preexisting, likely Triassic mafic arc crust and assimilation of metasedimentary wall rock either at depth or at the present level of emplacement. The high-Sr/Y magmatic rocks primarily represent recycling of isotopically juvenile, Triassic arc crust of the underthrusted Wallowa arc, rather than new Cretaceous additions to continental crust. However, the presence of mafic enclaves presents convincing evidence that mantle-derived basaltic magmas were emplaced prior to or contemporaneously with the high-Sr/Y suite, and these basaltic melts likely provided thermal energy to partially melt the lower crust. Furthermore, type 2 low-Sr/Y tonalites extend to more mafic and juvenile isotopic compositions; this indicates that they were derived from or mixed to a larger degree with mantle-derived magmas (cf. Fig. 13D). Deep-crustal magma mixing as an origin for the type 2 low-Sr/Y tonalites is also supported by numerical simulations of basalt diking that demonstrate the inefficiency of voluminous partial melting outside the lower crust (Dufek and Bergantz, 2005).

Studies of collisional orogenic belts commonly invoke erosion-driven upward rebound of depressed geothermal gradients and/or radioactive self-heating to partially melt the middle to lower crust (England and Thompson, 1984; Patiño Douce et al., 1990; Gerdes et al., 2000).

Time scales for partial melting by these mechanisms vary, but are typically tens of millions of years (Beaumont et al., 2004; Jamieson et al., 2004). The 7 m.y. time interval between collisional orogenesis and partial melting in the Blue Mountains province (154–147 Ma) is short and probably required advection of heat from mantle-derived melts in addition to heating from relaxation of geotherms to internally generate the temperatures required for partial melting (>900 °C), assuming equilibrium geothermal conditions prior to collision. One possibility is that mantle heat was supplied by mafic underplating generated by renewed subduction-related magmatism associated with reorganization of plate boundaries following arc-arc collision (cf. model in Schwartz et al., 2011b; Figs. 2A–2C). In this scenario, increased mantle power input during subduction resulted in the development of a MASH zone (melting, assimilation, storage, homogenization; Hildreth and Moorbath, 1988) at the lower crust–mantle transition, where underplated basalts mixed with lower crustal (Wallowa arc) partial melts. Figure 16 shows our conceptual view for the generation of the tonalite-granodiorite suite whereby the high-Sr/Y type 1 magmas are chiefly lower crustal partial melts with limited influence from basalt-crustal melt mixing. By contrast, low-Sr/Y type 2 magmas reflect greater mixing and homogenization with basaltic melts. Both type 1 and 2 magmas assimilated argillaceous wall rock at depth, during ascent or at the level of emplacement. Enclaves present in both type 1 and type 2 magmas likely represent injections of

a distinct mantle-derived low-Sr/Y magma, the source of which may have driven deep-crustal anatexis beneath the Bald Mountain batholith.

CONCLUSIONS

Magmatic construction of the Bald Mountain batholith occurred over ~15 m.y., commencing with the syncollisional emplacement of the low-Sr/Y (<40) norite-granite suite. This event included emplacement of the norite of Badger Butte (156.9 ± 1.4 Ma) and the granite of Anthony Butte (154.7 ± 1.3 Ma). Plutons of similar age occur throughout the Baker terrane and signify the waning stages of subduction-related magmatism associated with terminal arc-arc collision (Schwartz et al., 2011b) between the Wallowa and Olds Ferry island-arc terranes.

A second phase of postcollisional magmatism is characterized by the emplacement of tonalitic to granodioritic magmas from 147 to 141 Ma. The majority of these magmas (type 1) are high-Sr/Y (>40) tonalites and granodiorites that are postcollisional and have geochemical signatures consistent with dehydration–partial melting of garnet-bearing amphibolites, leaving behind a plagioclase-poor residue of garnet + amphibole + clinopyroxene. A second suite of lower Sr/Y (<40), augite-bearing tonalites (type 2) in the northernmost portion of the batholith has distinct geochemical characteristics and represents (1) mixing between a high-Sr/Y felsic magma and low-Sr/Y mafic magma, (2) mid-crustal (<1.0 GPa) partial melting of mafic crust leaving behind an amphibolite +

Hypothesized construction models for the tonalite-granodiorite suite (147–141 Ma)

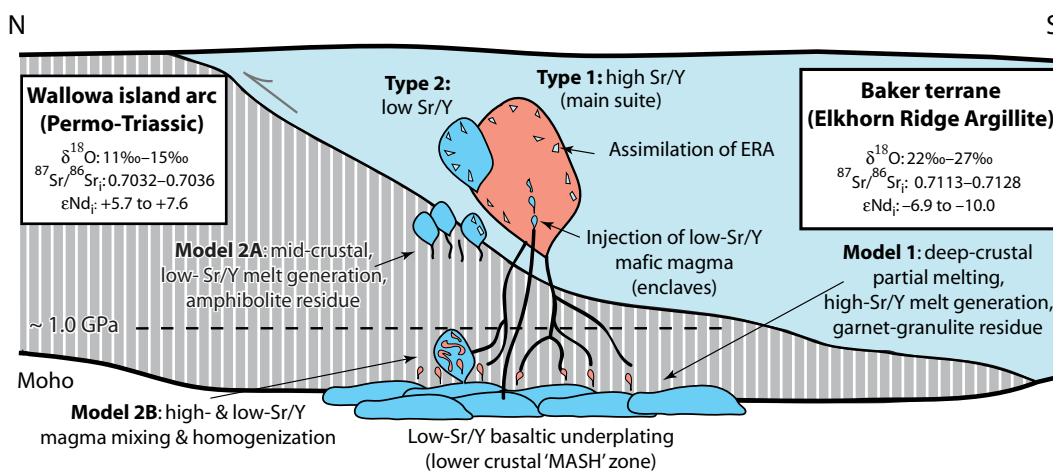


Figure 16. Detailed model for the generation of the tonalite-granodiorite suite of Bald Mountain batholith. High-Sr/Y rocks were generated by dehydration–partial melting of mafic arc crust in a lower crustal MASH zone (melting, assimilation, storage, homogenization; Hildreth and Moorbath, 1988) at >1.0 GPa pressure. Heat was supplied by mafic underplating of subduction-related magmas. During ascent through the Baker terrane, high-Sr/Y magmas assimilated high- $\delta^{18}\text{O}$ Elkhorn Ridge Argillite (ERA). Low-Sr/Y tonalites of the northernmost pluton represent mixing and homogenization with crustal and basaltic melts at depth or partial melts of Wallowa arc crust at intermediate depths.

plagioclase retrace, and/or (3) low-pressure fractionation of a basaltic magma.

The ubiquitous occurrence of mafic enclaves in both type 1 and type 2 tonalites and granodiorites suggests that mantle-derived mafic magmas were present during high-Sr/Y magma generation. No coeval mafic plutons have been identified at the current level of erosion; however, we speculate that these bodies may exist at depth and may have provided a heat source for lower crustal anatexis. The mafic enclaves may represent injections of mantle-derived basalts into tonalitic to granodioritic magma chambers. We suggest that increased mantle power associated with renewed subduction-related magmatism beginning ca. 147 Ma (Schwartz et al., 2011b) generated mafic enclaves and putative deep-crustal mafic magmas. This influx of basalt and heat triggered lower crustal partial melting of orogenically thickened Wallowa arc crust (Fig. 16). We also conclude that older Jurassic mafic plutons, such as the norite of Badger Butte, cannot be chemically related to the tonalite-granodiorite suite, and therefore are not considered an important component of arc construction from 147 to 141 Ma. This observation distinguishes norites in the Bald Mountain batholith from those exposed in other arc sections (e.g., Kohistan and Talkeetna; Garrido et al., 2006; Kelemen et al., 2003) where they are commonly interpreted as important cumulate components of subduction-related arc magmatism. We also note that all plutonic rocks in the Bald Mountain batholith, including the norite-granite suite and both type 1 and type 2 tonalites and granodiorites, show evidence for significant assimilation of metasedimentary wall rock (Elkhorn Ridge Argillite) either at depth and/or during ascent to shallow crustal pressures. We conclude that the observed pulse of type 1 high-Sr/Y magmas largely represents recycling of existing crust that was triggered by the addition of heat from underplated, subduction-related mafic magmas.

ACKNOWLEDGMENTS

We acknowledge discussions and comments by Mark L. Ferns, Art Snoke, and Cal Barnes. We thank Craig Grimes for assistance with sample preparation and for suggesting *in situ* analysis of zircons for $\delta^{18}\text{O}$. We also thank Brad Ito for keeping the SHRIMP-RG (sensitive high-resolution ion microprobe-reverse geometry) working so well and efficiently, and George Kamenov for assistance with Lu-Hf analyses. Noriko Kita and Jim Kern assisted in the Wisconsin Secondary Ion Mass Spectrometer Laboratory (WiscSIMS). We thank Mike Spicuzza for assistance with laser fluorination analyses of $\delta^{18}\text{O}$. We thank Harold Stowell for assistance with pseudosection modeling of the Elkhorn Ridge Argillite, and Jonathan Rivas and Brian Clements for assistance in the California State University Northridge LA-SF-ICPMS laboratory (laser ablation-sector field-inductively coupled plasma-mass spectrometry). The manuscript benefited greatly from reviews by Jon-

athan Miller, Diane Clemens-Knott, Associate Editor Rita Economos, and Science Editor Shanaka de Silva. Partial financial support for this work was provided by National Science Foundation (NSF) grant EAR-0911681 (to Schwartz), NSF grant EAR-0911735 (to Johnson), and a University of Houston-Downtown Organized Research Committee grant (to Johnson). WiscSIMS is partially supported by NSF grants EAR-0319230, EAR-0744079, and EAR-1053466.

REFERENCES CITED

- Alonso-Perez, R., Müntener, O., and Ulmer, P., 2009, Igneous garnet and amphibole fractionation in the roots of island arcs: Experimental constraints on andesitic liquids: *Contributions to Mineralogy and Petrology*, v. 157, p. 541–558, doi:10.1007/s00410-008-0351-8.
- Anderson, J.L., and Smith, D.R., 1995, The effect of temperature and oxygen fugacity on Al-in-hornblende barometry: *American Mineralogist*, v. 80, p. 549–559.
- Appleby, S.K., Graham, C.M., Gillespie, M.R., Hinton, R.W., Oliver, G.J.H., and Kelly, N.M., 2010, Do S-type granites commonly sample infracrustal sources? New results from an integrated O, U-Pb and Hf isotope study of zircon: *Contributions to Mineralogy and Petrology*, v. 160, p. 115–132, doi:10.1007/s00410-009-0469-3.
- Armstrong, R.L., Taubeneck, W.H., and Hales, P.O., 1977, Rb-Sr and K-Ar geochronometry of Mesozoic granitic rocks and their Sr isotopic composition, Oregon, Washington, and Idaho: *Geological Society of America Bulletin*, v. 88, p. 397–411, doi:10.1130/0016-7606(1977)88<397:RAKGOM>2.0.CO;2.
- Arth, J.G., Barker, F., Peterman, Z.E., and Friedman, I., 1978, Geochemistry of the gabbro-diorite-tonalite-trondhjemite suite of southwest Finland and its implications for the origin of tonalite and trondhjemite magmas: *Journal of Petrology*, v. 19, p. 289–316, doi:10.1093/ptrology/19.2.289.
- Ashley, R.P., 1995, Petrology and deformation history of the Burnt River Schist and associated plutonic rocks in the Burnt River Canyon area, northeastern Oregon, *in* Vallier, T.L., and Brooks, H.C., eds., *Geology of the Blue Mountains region Oregon, Idaho and Washington: petrology and tectonic evolution of pre-Tertiary rocks of the Blue Mountains region*: U.S. Geological Survey Professional Paper 1438, p. 457–495.
- Avé Lallemant, H.G., 1995, Pre-Cretaceous tectonic evolution of the Blue Mountains province, northeastern Oregon, *in* Vallier, T.L., and Brooks, H.C., eds., *Geology of the Blue Mountains region of Oregon, Idaho, and Washington: petrology and tectonic evolution of pre-Tertiary rocks of the Blue Mountains region*: U.S. Geological Survey Professional Paper 1438, p. 271–304.
- Bachmann, O., Oberli, F., Dungan, M.A., Meier, M., Mundil, R., and Fischer, H., 2007, $^{40}\text{Ar}/^{39}\text{Ar}$ and U-Pb dating of the Fish Canyon magmatic system, San Juan Volcanic field, Colorado: Evidence for an extended crystallization history: *Chemical Geology*, v. 236, p. 134–166, doi:10.1016/j.chemgeo.2006.09.005.
- Bacon, C.R., and Lowenstern, J.B., 2005, Late Pleistocene granodiorite source for recycled zircon and phenocrysts in rhyodacite lava at Crater Lake, Oregon: *Earth and Planetary Science Letters*, v. 233, p. 277–293, doi:10.1016/j.epsl.2005.02.012.
- Bacon, C.R., Persing, H.M., Wooden, J.L., and Ireland, T.R., 2000, Late Pleistocene granodiorite beneath Crater Lake caldera, Oregon, dated by ion microprobe: *Geology*, v. 28, p. 467–470, doi:10.1130/0091-7613(2000)28<467:LPGBCCL>2.0.CO;2.
- Barboni, M., and Schoene, B., 2014, Short eruption window revealed by absolute crystal growth rates in a granitic magma: *Nature Geoscience*, v. 7, p. 524–528, doi:10.1038/ngeo2185.
- Barnes, C.G., Petersen, S.W., Kistler, R.W., Murray, R.W., and Kays, M.A., 1996, Source and tectonic implications of tonalite-trondhjemite magmatism in the Klamath Mountains: *Contributions to Mineralogy and Petrology*, v. 123, p. 40–60, doi:10.1007/s004100050142.
- Barnes, C.G., Snoke, A.W., Harper, G.D., Frost, C.D., McFadden, R.R., Bushey, J.C., and Barnes, M.A.W., 2006, Arc plutonism following regional thrusting:

- Petrology and geochemistry of syn- and post-Nevadan plutons in the Siskiyou Mountains, Klamath Mountains province, California, *in* Snoke, A.W., and Barnes, C.G., eds., *Geological studies in the Klamath Mountains Province, California and Oregon: A volume in honor of William P. Irwin*: Geological Society of America Special Paper 410, p. 357–376, doi:10.1130/2006.2410(17).
- Barth, A.P., Feilen, A.D.G., Yager, S.L., Douglas, S.R., Wooden, J.L., Riggs, N.R., and Walker, J.D., 2012, Petrogenetic connections between ash-flow tuffs and a granodioritic to granitic intrusive suite in the Sierra Nevada arc, California: *Geosphere*, v. 8, p. 250–264, doi:10.1130/GES00737.1.
- Bateman, P.C., 1992, Plutonism in the central part of the Sierra Nevada batholith, California: U.S. Geological Survey Professional Paper 1483, 186 p.
- Beaumont, C., Jamieson, R.A., Nguyen, M.H., and Medvedev, S., 2004, Crustal channel flows; 1, Numerical models with applications to the tectonics of the Himalayan-Tibetan Orogen: *Journal of Geophysical Research*, v. 109, B06406, doi:10.1029/2003JB002809.
- Bowman, J.R., Moser, D.E., Valley, J.W., Wooden, J.L., Kita, N.T., and Mazdab, F., 2011, Zircon U-Pb isotope, $\delta^{18}\text{O}$ and trace element response to 80 m.y. of high temperature formation: *American Journal of Science*, v. 311, p. 719–772, doi:10.2475/09.2011.01.
- Brooks, H.C., and Vallier, T.L., 1978, Mesozoic rocks and tectonic evolution of eastern Oregon and western Idaho, *in* Howell, D.G., and McDougall, K.A., eds., *Mesozoic paleogeography of the western United States*: Los Angeles, California, Pacific Section, Society of Economic Paleontologists and Mineralogists, p. 133–145.
- Brown, S.J.A., and Fletcher, I.R., 1999, SHRIMP U-Pb dating of the preeruption growth history of zircons from the 340 ka Whakamaru Ignimbrite, New Zealand: Evidence for >250 k.y. magma residence times: *Geology*, v. 27, p. 1035–1038, doi:10.1130/0091-7613(1999)027<1035:SUPDOT>2.3.CO;2.
- Bryan, W.B., Finger, L.W., and Chayes, F., 1969, Estimating proportions in petrographic mixing equations by least squares approximation: *Science*, v. 163, p. 926–927, doi:10.1126/science.163.3870.926.
- Cecil, M.R., Rotberg, G., Ducea, M.N., Saleeby, J.B., and Gehrels, G.E., 2012, Magmatic growth and batholithic root development in the northern Sierra Nevada, California: *Geosphere*, v. 8, p. 592–606, doi:10.1130/GES00729.1.
- Charlier, B.L.A., Wilson, C.J.N., Lowenstern, J.B., Blake, S., van Calsteren, P.W., and Davidson, J.P., 2005, Magma generation at a large, hyperactive silicic volcano (Taupo, New Zealand) revealed by U-Th and U-Pb systematics in zircons: *Journal of Petrology*, v. 46, p. 3–32, doi:10.1093/ptrology/egh060.
- Cherniak, D.J., and Watson, E.B., 2003, Diffusion in zircon, *in* Hanchar, J.M., and Hoskin, P.W.O., eds., *Zircon: Reviews in Mineralogy and Geochemistry* Volume 53, p. 113–143.
- Cherniak, D.J., Hanchar, J.M., and Watson, E.B., 1997, Diffusion of tetravalent cations in zircon: *Contributions to Mineralogy and Petrology*, v. 127, p. 383–390, doi:10.1007/s004100050287.
- Chung, S.L., Liu, D.Y., Ji, J.Q., Chu, M.F., Lee, H.Y., Wen, D.J., Lo, C.H., Lee, T.Y., Qian, Q., and Zhang, Q., 2003, Adakites from continental collision zones: Melting of thickened lower crust beneath southern Tibet: *Geology*, v. 31, p. 1021–1024, doi:10.1130/G19796.1.
- Coleman, D.S., Gray, W., and Glazner, A.F., 2004, Rethinking the emplacement and evolution of zoned plutons: Geochronologic evidence for incremental assembly of the Tuolumne intrusive suite, California: *Geology*, v. 32, p. 433–436, doi:10.1130/G20220.1.
- DeCelles, P.G., Ducea, M.N., Kapp, P., and Zandt, G., 2009, Cyclicity in Cordilleran orogenic systems: *Nature Geoscience*, v. 2, p. 251–257, doi:10.1038/ngeo469.
- De Paoli, M.C., Clarke, G.L., Klepeis, K.A., Allibone, A.H., and Turnbull, I.M., 2009, The eclogite-granulite transition: Mafic and intermediate assemblages at Breaksea Sound, New Zealand: *Journal of Petrology*, v. 50, p. 2307–2343, doi:10.1093/ptrology/egp078.
- de Silva, S.L., and Gosnold, W.D., 2007, Episodic construction of batholiths: Insights from the spatiotemporal development of an ignimbrite flare-up: *Journal of*

- Volcanology and Geothermal Research, v. 167, p. 320–335, doi:10.1016/j.jvolgeores.2007.07.015.
- Dhuime, B., Hawkesworth, C., and Cawood, P., 2011, When continents formed: Science, v. 331, p. 154–155, doi:10.1126/science.1201245.
- Dickinson, W.R., 1979, Mesozoic forearc basin in central Oregon: Geology, v. 7, p. 166–170.
- Dickinson, W.R., and Thayer, T.P., 1978, Paleographic and paleotectonic implications of Mesozoic stratigraphy and structure in the John Day inlier of central Oregon, in Howell, D.G., and McDougall, K.A., eds., Mesozoic paleogeography of the western United States: Los Angeles, California, Pacific Section, Society of Economic Paleontologists and Mineralogists, p. 147–161.
- Dickinson, W.R., Helmold, K.P., and Stein, J.A., 1979, Mesozoic lithic sandstones in central Oregon: Journal of Sedimentary Research, v. 49, p. 501–516, doi:10.1306/212F777A-2B24-11D7-8648000102C1865D.
- Drummond, M., and Defant, M., 1990, A model for trondhjemite-tonalite-dacite genesis and crystal growth via slab melting: Archean to modern comparisons: Journal of Geophysical Research, v. 95, p. 21503–21521, doi:10.1029/JB095iB13p21503.
- Ducea, M.N., 2001, The California arc: Thick granitic batholiths, eclogitic residues, lithospheric-scale thrusting, and magmatic flare-ups: GSA Today, v. 11, p. 4–10, doi:10.1130/1052-5173(2001)011<0004:TCATGB>2.0.CO;2.
- Ducea, M.N., 2002, Constraints on the bulk composition and root foundering rates of continental arcs: A California arc perspective: Journal of Geophysical Research, v. 107, p. ECV 15-1–ECV 15-13, doi:10.1029/2001JB000643.
- Ducea, M.N., and Barton, M.D., 2007, Igniting flare-up events in Cordilleran arcs: Geology, v. 35, p. 1047–1050, doi:10.1130/G23898A.1.
- Dufek, J., and Bergantz, G.W., 2005, Lower crustal magma genesis and preservation: A stochastic framework for the evaluation of basalt-crust interaction: Journal of Petrology, v. 46, p. 2167–2195, doi:10.1093/petrology/egi049.
- England, P.C., and Thompson, A.B., 1984, Pressure-temperature-time paths of regional metamorphism I: Heat transfer during the evolution of regions of thickened continental crust: Journal of Petrology, v. 25, p. 894–928, doi:10.1093/petrology/25.4.894.
- Ferns, M.L., and Brooks, H.C., 1995, The Bourne and Greenhorn subterranean of the Baker terrane, northeastern Oregon: Implications for the evolution of the Blue Mountains island-arc system, in Vallier, T.L., and Brooks, H.C., eds., Geology of the Blue Mountains region of Oregon, Idaho, and Washington: petrology and tectonic evolution of pre-Tertiary rocks of the Blue Mountains region: U.S. Geological Survey Professional Paper 1438, p. 331–358.
- Ferns, M.L., and Taubeneck, W.H., 1994, Geology and mineral resources of the Limber Jim Creek quadrangle, Union County, Oregon: Oregon Department of Geology and Mineral Industries Geological Map Series GMS-82, scale 1:24,000.
- Ferns, M.L., Brooks, H.C., and Ducette, J., 1982, Geology and mineral resources map of the Mt Ireland quadrangle, Baker and Grant Counties, Oregon: Oregon Department of Geology and Mineral Industries Geological Map Series GMS-22, scale 1:24,000.
- Frost, B.R., Barnes, C.G., Collins, W.J., Arculus, R.J., Ellis, D.J., and Frost, C.D., 2001, A geochemical classification for granitic rocks: Journal of Petrology, v. 42, p. 2033–2048, doi:10.1093/petrology/42.11.2033.
- Garrido, C.J., Bodinier, J.-L., Burg, J.-P., Zeilinger, S.S.H., Dawood, H., Chaudhry, M.N., and Gervilla, F., 2006, Petrogenesis of mafic garnet granulite in the lower crust of the Kohistan paleo-arc complex (northern Pakistan): Implications for intra-crustal differentiation of island arcs and generation of continental crust: Journal of Petrology, v. 47, p. 1873–1914, doi:10.1093/petrology/egi030.
- Gerdes, A., Henk, A., and Wörner, G., 2000, Post-collisional granite generation and HT/LP metamorphism by radiogenic heating: The Variscan South Bohemian Batholith: Geological Society of London Journal, v. 157, p. 577–587, doi:10.1144/jgs.157.3.577.
- Getty, S.R., Selverstone, J., Wernicke, B.P., Jacobsen, S.B., and Aliberti, E., 1993, Sm-Nd dating of multiple garnet growth events in an arc-continent collision zone, northwestern US Cordillera: Contributions to Mineralogy and Petrology, v. 115, p. 45–57, doi:10.1007/BF00712977.
- Ghiorso, M.S., and Sack, R.O., 1995, Chemical mass transfer in magmatic processes. IV A revised and internally consistent thermodynamic model for the interpolation and extrapolation of liquid-solid equilibria in magmatic systems at elevated temperatures and pressures: Contributions to Mineralogy and Petrology, v. 119, p. 197–212, doi:10.1007/BF00307281.
- Glazner, A.F., Bartley, J.M., Coleman, D.S., Gray, W., and Taylor, R.Z., 2004, Are plutons assembled over millions of years by amalgamation from small magma chambers?: GSA Today, v. 14, no. 4, p. 4–11, doi:10.1130/1052-5173(2004)014<0004:APAOMO>2.0.CO;2.
- Glazner, A.F., Coleman, D.S., and Bartley, J.M., 2008, The tenuous connection between high-silica rhyolites and granodiorite plutons: Geology, v. 36, p. 183–186, doi:10.1130/G24496A.1.
- Gromet, P., and Silver, L.T., 1987, REE variations across the Peninsular Ranges Batholith: Implications for batholithic petrogenesis and crustal growth in magmatic arcs: Journal of Petrology, v. 28, p. 75–125, doi:10.1093/petrology/28.1.75.
- Guo, Z.F., Wilson, M., and Liu, J.Q., 2007a, Post-collisional adakites in south Tibet: Products of partial melting of subduction-modified lower crust: Lithos, v. 96, p. 205–224, doi:10.1016/j.lithos.2006.09.011.
- Guo, F., Nakamura, E., Fan, W., Kobayoshi, K., and Li, C., 2007b, Generation of Palaeocene adakitic andesites by magma mixing: Yanji area, NE China: Journal of Petrology, v. 48, p. 661–692, doi:10.1093/petrology/egi077.
- Harmon, R.S., and Hoefs, J., 1995, Oxygen isotope heterogeneity of the mantle deduced from global ^{18}O systematics of basalts from different geotectonic settings: Contributions to Mineralogy and Petrology, v. 120, p. 95–114, doi:10.1007/BF00311010.
- Harrison, T.M., and Watson, E.B., 1984, The behavior of apatite during crustal anatexis: Equilibrium and kinetic considerations: Geochimica et Cosmochimica Acta, v. 48, p. 1467–1477, doi:10.1016/0016-7037(84)90403-4.
- Hildreth, W., and Moorbath, S., 1988, Crustal contributions to arc magmatism in the Andes of central Chile: Contributions to Mineralogy and Petrology, v. 98, p. 455–489, doi:10.1007/BF00372365.
- Holland, T., and Blundy, J., 1994, Non-ideal interactions in calcic amphiboles and their bearing on amphibole-plagioclase thermometry: Contributions to Mineralogy and Petrology, v. 116, p. 433–447, doi:10.1007/BF00310910.
- Hooper, P.R., Houseman, M.D., Beane, J.E., Cafrey, G.M., Eng, K.R., Scribner, J.V., and Watkinson, A.J., 1995, Geology of the northern part of the Ironside Inlier, northeastern Oregon in Vallier, T.L., and Brooks, H.C., eds., Geology of the Blue Mountains region of Oregon, Idaho, and Washington: petrology and tectonic evolution of pre-Tertiary rocks of the Blue Mountains region: U.S. Geological Survey Professional Paper 1438, p. 415–455.
- Ingram, S.B., 2012, U-Pb zircon and monazite geochronology and Hf isotope geochemistry of Neocadian and early Alleghanian plutonic rocks in the Alabama eastern Blue Ridge, Southern Appalachian Mountains [M.S. thesis]: Tuscaloosa, University of Alabama, 80 p.
- Jamieson, R.A., Beaumont, C., Medvedev, S., and Nguyen, M.H., 2004, Crustal channel flows: 2. Numerical models with implications for metamorphism in the Himalayan-Tibetan Orogen: Journal of Geophysical Research, v. 109, doi:10.1029/2003JB002811.
- Johnson, K., and Schwartz, J.J., 2009, Overview of Jurassic–Cretaceous magmatism in the Blue Mountains Province (NE Oregon & W Idaho): Insights from New Pb/U (SHRIMP-RG) age determinations: Geological Society of America Abstracts with Programs, v. 41, no. 7, p. 182.
- Johnson, K., Barnes, C.G., and Miller, C.A., 1997, Petrology, geochemistry, and genesis of high-Al tonalite and trondhjemites of the Cornucopia stock, Blue Mountains, northeastern Oregon: Journal of Petrology, v. 38, p. 1585–1611, doi:10.1093/petroj/38.11.1585.
- Kelemen, P.B., Hanghøj, K., and Greene, A.R., 2003, One view of the geochemistry of subduction-related magmatic arcs, with an emphasis on primitive andesite and lower crust, in Rudnick, R.L., ed., Treatise on geochemistry, Volume 3: The crust: Amsterdam, Elsevier, p. 593–659, doi:10.1016/B0-08-043751-6/03035-8.
- Kemp, A.I.S., Hawkesworth, C.J., Foster, G.L., Paterson, B.A., Woodhead, J.D., Hergt, J.M., Gray, C.M., and Whitehouse, M.J., 2007, Magmatic and crustal differentiation history of granitic rocks from Hf-O isotopes in zircon: Science, v. 315, p. 980–983, doi:10.1126/science.1136154.
- Kimbrough, D.L., Smith, D.P., Mahoney, J.B., Moore, T.E., Grove, M., Gastil, R.G., Ortega-Rivera, A., and Fanning, C.M., 2001, Forearc-basin sedimentary response to rapid Late Cretaceous batholith emplacement in the Peninsular Ranges of southern and Baja California: Geology, v. 29, p. 491–494, doi:10.1130/0091-7613(2001)029<0491:FBSRTR>2.0.CO;2.
- King, E.M., and Valley, J.W., 2000, The source, magmatic contamination, and alteration of the Idaho Batholith: Contributions to Mineralogy and Petrology, v. 142, p. 72–88, doi:10.1007/s004100100278.
- Kurz, G.A., Schmidt, M.D., Northrup, C.J., and Vallier, T.L., 2012, U-Pb geochronology and geochemistry of intrusive rocks from the Cougar Creek Complex, Wallowa arc terrane, Blue Mountains province, Oregon-Idaho: Geological Society of America Bulletin, v. 124, p. 578–595, doi:10.1130/B30452.1.
- Lackey, J., Valley, J., and Saleeby, J., 2005, Supracrustal input to magmas in the deep crust of Sierra Nevada batholith: Evidence from high $\delta^{18}\text{O}$ zircon: Earth and Planetary Science Letters, v. 235, p. 315–330, doi:10.1016/j.epsl.2005.04.003.
- Lackey, J.S., Valley, J.W., and Hinkle, H.J., 2006, Deciphering the source and contamination history of peraluminous magmas using $\delta^{18}\text{O}$ of accessory minerals: Examples from garnet-bearing plutons of the Sierra Nevada batholith: Contributions to Mineralogy and Petrology, v. 151, p. 20–44, doi:10.1007/s00410-005-0043-6.
- Lackey, J.S., Valley, J.W., Chen, J.H., and Stockli, D.F., 2008, Dynamic magma systems, crustal recycling, and alteration in the central Sierra Nevada Batholith: The oxygen isotope record: Journal of Petrology, v. 49, p. 1397–1426, doi:10.1093/petrology/egn030.
- LaMaskin, T.A., Schwartz, J.J., Dorsey, R.J., Snoko, A.W., Johnson, K., and Vervoort, J.D., 2009, Mesozoic sedimentation, magmatism, and tectonics in the Blue Mountains Province, northeastern Oregon, in O'Connor, J.E., et al., eds., Volcanoes to vineyards: Geologic field trips through the dynamic landscape of the Pacific Northwest: Geological Society of America Field Guide 15, p. 187–202, doi:10.1130/2009.fld015(09).
- Langmuir, C.H., 1989, Geochemical consequences of in situ crystallization: Nature, v. 340, p. 199–205, doi:10.1038/340199a0.
- Lee, C.-T.A., Cheng, X., and Horodyskyj, U., 2006, The development and refinement of continental arcs by primary basaltic magmatism, garnet pyroxenite accumulation, basaltic recharge and delamination: Insights from the Sierra Nevada, California: Contributions to Mineralogy and Petrology, v. 151, p. 222–242, doi:10.1007/s00410-005-0056-1.
- Lipman, P.W., 2007, Incremental assembly and prolonged consolidation of Cordilleran magma chambers: Evidence from the Southern Rocky Mountain volcanic field: Geosphere, v. 3, p. 42–70, doi:10.1130/GES00061.1.
- Macpherson, C.G., Dreher, S.T., and Thirlwall, M.F., 2006, Adakites without slab melting: High pressure differentiation of island arc magma, Mindanao, the Philippines: Earth and Planetary Science Letters, v. 243, p. 581–593, doi:10.1016/j.epsl.2005.12.034.
- Mahan, K.H., Bartley, J.M., Coleman, D.S., Glazner, A.F., and Carl, B.S., 2003, Sheeted intrusion of the synkinematic McDoogie pluton, Sierra Nevada, California: Geological Society of America Bulletin, v. 115, p. 1570–1582, doi:10.1130/B22083.1.
- Matzel, J.E.P., Bowring, S.A., and Miller, R.B., 2006, Time scales of pluton construction at differing crustal levels:

Cordilleran batholith construction and high-Sr/Y magmatic pulses

- Examples from the Mount Stuart and Tenpeak intrusions, North Cascades, Washington: Geological Society of America Bulletin, v. 118, p. 1412–1430, doi:10.1130/B25923.1.
- McKay, M., 2011, Pressure-temperature-time paths, prograde garnet growth, and protholite of tectonites from a polydeformational, polymetamorphic terrane: Salmon River suture zone, west-central Idaho [M.S. thesis]: Tuscaloosa, University of Alabama, 135 p.
- Memeti, V., Paterson, S., Matzel, J., Mundil, R., and Okaya, D., 2010, Magmatic lobes as “snapshots” of magma chamber growth and evolution in large, composite batholiths: An example from the Tuolumne intrusion, Sierra Nevada, California: Geological Society of America Bulletin, v. 122, p. 1912–1931, doi:10.1130/B30004.1.
- Michel, J., Baumgartner, L., Putlitz, B., Schaltegger, U., and Ovtcharova, M., 2008, Incremental growth of the Patagonian Torres del Paine laccolith over 90 k.y.: Geology, v. 36, p. 459–462, doi:10.1130/G24546A.1.
- Miller, J.S., and Wooden, J.L., 2004, Residence, resorption and recycling of zircons in Devils Kitchen rhyolite, Coso Volcanic Field, California: Journal of Petrology, v. 45, p. 2155–2170, doi:10.1093/petrology/egh051.
- Miller, J.S., Matzel, J.E.P., Miller, C.F., Burgess, S.D., and Miller, R.B., 2007, Zircon growth and recycling during the assembly of large, composite arc plutons: Journal of Volcanology and Geothermal Research, v. 167, p. 282–299, doi:10.1016/j.jvolgeores.2007.04.019.
- Miller, R.B., and Paterson, S.R., 2001, Construction of mid-crustal sheeted plutons: Examples from the North Cascades, Washington: Geological Society of America Bulletin, v. 113, p. 1423–1442, doi:10.1130/0016-7606(2001)113<1423:COMCSP>2.0.CO;2.
- Oberli, F., Meier, M., Berger, A., Rosenberg, C.L., and Gieré, R., 2004, U-Th-Pb and ²³⁰Th/²³⁸U disequilibrium isotope systematics: Precise accessory mineral chronology and melt evolution tracing in the Alpine Bergell intrusion: Geochimica et Cosmochimica Acta, v. 68, p. 2543–2560, doi:10.1016/j.gca.2003.10.017.
- Page, F.Z., Ushikubo, T., Kita, N.T., Riciputi, L.R., and Valley, J.W., 2007, High precision oxygen isotope analysis of picogram samples reveals 2-μm gradients and slow diffusion in zircon: American Mineralogist, v. 92, p. 1772–1775, doi:10.2138/am.2007.2697.
- Paterson, S.R., Okaya, D., Memeti, V., Economos, R., and Miller, R.B., 2011, Magma addition and flux calculations of incrementally constructed magma chambers in continental margin arcs: Combined field, geochronologic, and thermal modeling studies: Geosphere, v. 7, p. 1439–1468, doi:10.1130/GES00696.1.
- Patiño Douce, A.E., Humphreys, E.D., and Johnston, A.D., 1990, Anatexis and metamorphism in tectonically thickened continental crust exemplified by the Sevier hinterland, western North America: Earth and Planetary Science Letters, v. 97, p. 290–315, doi:10.1016/0012-821X(90)90048-3.
- Petford, N., and Atherton, M., 1996, Na-rich partial melts from newly underplated basaltic crust: the Cordillera Blanca Batholith, Peru: Journal of Petrology, v. 37, p. 1491–1521, doi:10.1093/petrology/37.6.1491.
- Rapp, R.P., 1995, Amphibole-out phase-boundary in partially melted metabasalt, its control over liquid fraction and composition, and source permeability: Journal of Geophysical Research, v. 100, p. 15601–15610, doi:10.1029/95JB00913.
- Rapp, R.P., and Watson, E.B., 1995, Dehydration melting of metabasalt at 8–32 kbar: Implications for continental growth and crust-mantle recycling: Journal of Petrology, v. 36, p. 891–931, doi:10.1093/petrology/36.4.891.
- Rapp, R.P., Watson, E.B., and Miller, C.F., 1991, Partial melting of amphibolite/eclogite and the origin of Archean trondhjemitic and tonalites: Precambrian Research, v. 51, p. 1–25, doi:10.1016/0301-9268(91)90092-O.
- Reid, M.R., 2014, Timescales of magma transfer and storage in the crust, in Rudnick, R.L., ed., Treatise on geochemistry: Volume 4: The crust: (second edition): Amsterdam, Elsevier, p. 181–201, doi:10.1016/B978-0-08-095975-7.00305-3.
- Reid, M.R., and Coath, C.D., 2000, In situ U-Pb ages of zircons from the Bishop Tuff: No evidence for long crystal residence times: Geology, v. 28, p. 443–446, doi:10.1130/0091-7613(2000)28<443:ISUAOZ>2.0.CO;2.
- Reid, M.R., Coath, C.D., Mark Harrison, T., and McKeegan, K.D., 1997, Prolonged residence times for the youngest rhyolites associated with Long Valley Caldera: ²³⁰Th-²³⁸U ion microprobe dating of young zircons: Earth and Planetary Science Letters, v. 150, p. 27–39, doi:10.1016/S0012-821X(97)00077-0.
- Rushmer, T., 1991, Partial melting of two amphibolites: Contrasting experimental results under fluid-absent conditions: Contributions to Mineralogy and Petrology, v. 107, p. 41–59, doi:10.1007/BF00311184.
- Saleeby, J., Ducea, M.N., Busby, C., Nadin, E., and Wetmore, P.H., 2008, Chronology of pluton emplacement and regional deformation in the southern Sierra Nevada batholith, California, in Wright, J.E., and Shervais, J.W., eds., Ophiolites, arcs, and batholiths: A tribute to Cliff Hopson: Geological Society of America Special Paper 438, p. 397–427, doi:10.1130/2008.2438(14).
- Schmitt, A.K., Lindsay, J.M., de Silva, S., and Trumbull, R.B., 2003, U-Pb zircon chronostratigraphy of early Pliocene ignimbrites from La Pacana, north Chile: Implications for the formation of stratified magma chambers: Journal of Volcanology and Geothermal Research, v. 120, p. 43–53, doi:10.1016/S0377-0273(02)00359-1.
- Schwartz, J.J., Snoke, A.W., Frost, C.D., Barnes, C.G., Gromet, L.P., and Johnson, K., 2010, Analysis of the Wallowa-Baker terrane boundary: Implications for tectonic accretion in the Blue Mountains province, northeastern Oregon: Geological Society of America Bulletin, v. 122, p. 517–536, doi:10.1130/B26493.1.
- Schwartz, J.J., Snoke, A.W., Cordey, F., Johnson, K., Frost, C.D., Barnes, C.G., LaMaskin, T.A., and Wooden, J.L., 2011a, Late Jurassic magmatism, metamorphism and deformation in the Blue Mountains province, northeast Oregon: Geological Society of America Bulletin, v. 123, p. 2083–2111, doi:10.1130/B30327.1.
- Schwartz, J.J., Johnson, K., Miranda, E.A., and Wooden, J.L., 2011b, The generation of high Sr/Y plutons following Late Jurassic arc-arc collision, Blue Mountains province, NE Oregon: Lithos, v. 126, p. 22–41, doi:10.1016/j.lithos.2011.05.005.
- Selverstone, J., Wernicke, B., and Aliberti, E.A., 1992, Intracontinental subduction and hinged unroofing along the Salmon River suture zone, west central Idaho: Tectonics, v. 11, p. 124–144, doi:10.1029/91TC02418.
- Sen, C., and Dunn, T., 1994, Dehydration melting of a basaltic composition amphibolites at 1.5 and 2.0 GPa: Implications for the origin of adakites: Contributions to Mineralogy and Petrology, v. 117, p. 394–409, doi:10.1007/BF00307273.
- Shand, S.J., 1947, Eruptive rocks (third edition): New York, John Wiley, 444 p.
- Silberling, N.J., Jones, D.L., Blake, M.C., and Howell, D.G., 1987, Lithotectonic terrane map of the western conterminous United States: U.S. Geological Survey Miscellaneous United States Field Studies Map MF-1874-C, scale 1:250,000, 20 p.
- Spera, F.J., and Bohrsen, W.A., 2002, Energy-constrained open-system magmatic processes III: Energy-constrained recharge, assimilation and fractional crystallization (EC-RAFC): Geochemistry, Geophysics, Geosystems, v. 3, no. 12, p. 1–20, doi:10.1029/2002GC000315.
- Sun, S.S., and McDonough, W.F., 1989, Chemical and isotopic systematics of oceanic basalts; implications for mantle composition and processes, in Saunders, A.D., and Norry, M.J., eds., Magmatism in the ocean basins: Geological Society of London Special Publication 42, p. 313–345, doi:10.1144/GSL.SP.1989.042.01.19.
- Taubeneck, W.H., 1957, Geology of the Elkhorn Mountains, northeastern Oregon; Bald Mountain batholith: Geological Society of America Bulletin, v. 68, p. 181–238, doi:10.1130/0016-7606(1957)68[181:GOTEMN]2.0.CO;2.
- Taubeneck, W.H., 1995, A closer look at the Bald Mountain batholith, Elkhorn Mountains, and some comparisons with the Wallowa batholith, Wallowa Mountains, northeastern Oregon, in Vallier, T.L., and Brooks, H.C., eds., Geology of the Blue Mountains region of Oregon, Idaho, and Washington; petrology and tectonic evolution of pre-Tertiary rocks of the Blue Mountains region: U.S. Geological Survey Professional Paper 1438, p. 45–123.
- Tulloch, A.J., and Kimbrough, D.L., 2003, Paired plutonic belts in convergent margins and the development of high Sr/Y magmatism: Peninsular Ranges batholith of Baja-California and Median batholith of New Zealand, in Johnson, S.E., et al., eds., Tectonic evolution of northwestern México and the southwestern USA: Geological Society of America Special Paper 374, p. 275–295, doi:10.1130/0-8137-2374-4.275.
- Valley, J.W., 2003, Oxygen isotopes in zircon, in Hanchar, J.M., and Hoskin, P.W.O., eds., Zircon: Reviews in Mineralogy and Geochemistry Volume 53, p. 343–385, doi:10.2113/0530343.
- Vallier, T.L., 1995, Petrology of pre-Tertiary igneous rocks in the Blue Mountains region of Oregon, Idaho, and Washington: Implications for the geologic evolution of a complex island arc, in Vallier, T.L., and Brooks, H.C., eds., Geology of the Blue Mountains region of Oregon, Idaho, and Washington; petrology and tectonic evolution of pre-Tertiary rocks of the Blue Mountains region: U.S. Geological Survey Professional Paper 1438, p. 125–209.
- Vazquez, J.A., and Reid, M.R., 2002, Time scales of magma storage and differentiation of voluminous high-silica rhyolites at Yellowstone caldera, Wyoming: Contributions to Mineralogy and Petrology, v. 144, p. 274–285, doi:10.1007/s00410-002-0400-7.
- Vazquez, J.A., and Reid, M.R., 2004, Probing the accumulation history of the voluminous Toba magma: Science, v. 305, p. 991–994, doi:10.1126/science.1096994.
- Vervoort, J.D., Patchett, P.J., Blichert-Toft, J., and Albarède, F., 1999, Relationships between Lu-Hf and Sm-Nd isotopic systems in the global sedimentary system: Earth and Planetary Science Letters, v. 168, p. 79–99, doi:10.1016/S0012-821X(99)00047-3.
- Walker, B.A., Miller, C.F., Lowery Claiborne, L., Wooden, J.L., and Miller, J.S., 2007, Geology and geochronology of the Spirit Mountain batholith, southern Nevada: Implications for timescales and physical processes of batholith construction: Journal of Volcanology and Geothermal Research, v. 167, p. 239–262, doi:10.1016/j.jvolgeores.2006.12.008.
- Walker, N.W., 1989, Early Cretaceous initiation of post-tectonic plutonism and the age of the Connor Creek fault, northeastern Oregon: Geological Society of America Abstracts with Programs, v. 21, no. 5, p. 155.
- Walker, N.W., 1995, Tectonic implications of U-Pb zircon ages of the Canyon Mountain complex, Sparta complex, and related metaplutonic rocks of the Baker terrane, northeastern Oregon, in Vallier, T.L., and Brooks, H.C., eds., Geology of the Blue Mountains region of Oregon, Idaho, and Washington; petrology and tectonic evolution of pre-Tertiary rocks of the Blue Mountains region: U.S. Geological Survey Professional Paper 1438, p. 247–269.
- Watson, E.B., and Harrison, T.M., 1983, Zircon saturation revisited: Temperature and composition effects in a variety of crustal magma types: Earth and Planetary Science Letters, v. 64, p. 295–304, doi:10.1016/0012-821X(83)90211-X.
- Winther, K.T., and Newton, R.C., 1991, Experimental melting of hydrous low-K tholeiite: evidence on the origin of Archean cratons: Geological Society of Denmark Bulletin, v. 39, p. 213–228.
- Wolf, M.B., and Wyllie, P.J., 1993, Garnet growth during amphibolite anatexis: Implications of a garnetiferous restite: Journal of Geology, v. 101, p. 357–373, doi:10.1086/648229.
- Wolf, M.B., and Wyllie, P.J., 1994, Dehydration-melting of amphibolite at 18 kbar: The effects of temperature and time: Contributions to Mineralogy and Petrology, v. 115, p. 369–383, doi:10.1007/BF00320972.

Geosphere

Time scales and processes of Cordilleran batholith construction and high-Sr/Y magmatic pulses: Evidence from the Bald Mountain batholith, northeastern Oregon

Joshua J. Schwartz, Kenneth Johnson, Paul Mueller, John Valley, Ariel Strickland and Joseph L. Wooden

Geosphere 2014;10;1456-1481
doi: 10.1130/GES01033.1

Email alerting services click www.gsapubs.org/cgi/alerts to receive free e-mail alerts when new articles cite this article

Subscribe click www.gsapubs.org/subscriptions/ to subscribe to Geosphere

Permission request click <http://www.geosociety.org/pubs/copyrt.htm#gsa> to contact GSA

Copyright not claimed on content prepared wholly by U.S. government employees within scope of their employment. Individual scientists are hereby granted permission, without fees or further requests to GSA, to use a single figure, a single table, and/or a brief paragraph of text in subsequent works and to make unlimited copies of items in GSA's journals for noncommercial use in classrooms to further education and science. This file may not be posted to any Web site, but authors may post the abstracts only of their articles on their own or their organization's Web site providing the posting includes a reference to the article's full citation. GSA provides this and other forums for the presentation of diverse opinions and positions by scientists worldwide, regardless of their race, citizenship, gender, religion, or political viewpoint. Opinions presented in this publication do not reflect official positions of the Society.

Notes